The Dual Molecular Identity of Vestibular Kinocilia: Bridging Structural and Functional Traits of Primary and Motile Cilia

Zhenhang Xu[1,2]†, Amirrasoul Tavakoli[3]†, Samadhi Kulasooriya[1], Huizhan Liu[1], Shu Tu[1], Celia Bloom[1], Yi Li[1,4], Jian Zuo[1], Litao Tao[1], Bechara Kachar[3*], David Z. He[1*]

[1]Department of Biomedical Sciences, Creighton University, Omaha, Nebraska 68178
[2]Department of Otorhinolaryngology-Head and Neck Surgery, Xiangya Hospital, Central South University, Changsha, China
[3]Section of Cell Biology, National Institute of Deafness and Other Communication Disorders, National Institutes of Health, Bethesda, Maryland
[4]Department of Otorhinolaryngology – Head and Neck Surgery, Beijing Tongren Hospital, Capital Medical University, Beijing, China

†These authors contribute equally to the work.

Bechara Kachar: kacharb@nidcd.nih.gov
David Z. He: hed@creighton.edu

ABSTRACT
Vestibular hair cells (HCs) detect head motion and orientation by transducing mechanical forces generated by gravity and acceleration into neural signals. This mechanotransduction is mediated by the hair bundle, which comprises stereocilia and a kinocilium—the latter considered a specialized form of primary cilium. To investigate its characteristics, we performed single-cell RNA sequencing on 1,522 adult vestibular and cochlear HCs. Our analysis revealed an enrichment of genes associated with motile cilia in vestibular HCs, particularly those linked to the axonemal repeat complex, a defining structural feature of motile cilia. Similar axonemal-related genes were identified in zebrafish and human vestibular HCs, highlighting a conserved molecular composition of kinocilia across vertebrate species. Immunostaining confirmed the expression of key motile cilia markers—including CCDC39, CCDC40, DNAH5, and DNAH6—in vestibular kinocilia. Live imaging of bullfrog saccular and mouse crista HCs revealed spontaneous kinociliary motion that drove oscillations of the hair bundle. Together, these findings establish the kinocilium as a distinct organelle with molecular hallmarks of motile cilia and suggest it functions as an active, force-generating vestibular hair bundle component, potentially influencing mechanosensitivity of HCs.

INTRODUCTION

The mammalian inner ear contains auditory and vestibular end organs to detect sound and motion respectively. Hair cells (HCs), the receptor cells in the inner ear, transduce mechanical stimulus (sound or head movement) into receptor potential. The auditory sensory epithelium in the cochlea contains two types of HCs, the inner and outer HCs (IHCs and OHCs). The vestibular end organs comprise two otolith organs (utricular and saccular maculae) and three cristae associated with semicircular canals. Similar to the cochlea, the vestibular sensory epithelium consists of two types of HCs known as type I and type II based on morphology, physiology, and innervation (Eatock et al., 1998; Eatock and Songer, 2011).

Although mechanotransduction is a shared feature of all HCs, mammalian cochlear and vestibular HCs differ in morphology and function. One key difference lies in the structure of the hair bundle, which harbors specialized machinery for mechanotransduction. The hair bundle of adult vestibular HCs encompasses tightly connected actin-rich stereocilia and a microtubule-based kinocilium via lateral links, whereas cochlear HCs lose the kinocilia during HC maturation (Leibovici et al., 2005). Kinocilia are highly conserved in non-mammalian vertebrates (Leibovici et al., 2005) and play a pivotal role in establishing hair bundle polarity and mediating Hedgehog and WNT signaling during HC development (Moon et al., 2020; Shi et al., 2022). Despite possessing features of motile cilia such as the canonical “9+2” microtubule arrangement, the kinocilium has long been regarded as a specialized primary cilium (Kikuchi et al., 1989; Wang and Zhou, 2021). While the kinocilium has been implicated in bundle stiffness and mechano-sensitivity (Baird, 1994; Kindt et al., 2012; Spoon and Grant, 2011), the molecular basis and function of this unique organelle in adult vestibular HCs remain unknown.

In the current study we utilized single-cell RNA-sequencing (scRNA-seq) to examine the transcriptomes of 1,522 HCs isolated from cochlear and vestibular sensory epithelia from adult CBA/J mice. Comparisons of the molecular profiles identified novel marker genes as well as shared and unique genes associated with mechanotransduction, ion channels, and pre- and post-synaptic structures in the four HC types (IHCs, OHCs, type I and type II). Notably, our analysis revealed a significant enrichment of genes related to primary and motile cilia in vestibular HCs, particularly those linked to the 96-nm axonemal repeat complex, a hallmark feature of motile cilia. Similar axonemal-related genes were also detected in zebrafish HCs and human vestibular HCs. We utilized transmission electron microscopy (TEM) to examine ultrastructure of kinocilia and immunostaining to detect expression of key motile cilia proteins in vestibular HCs. We used live imaging to examine kinocilia motion in bullfrog saccular HCs and mouse crista ampullaris. We modeled the atomic architecture of the 96-nm repeat, the core framework of the kinocilium axoneme. Together, our comprehensive approach uncovers kinocilia as a unique organelle with a molecular composition of both primary and motile cilia and implicates a kinocilium-driven process to modulate hair bundle dynamics in vertebrate vestibular HCs. In addition, our transcriptomic analysis provides new insight into molecular mechanisms underlying phenotypical differences among the four different HC types in the adult mouse inner ear.

RESULTS

Solitary cells were isolated from the whole basilar membrane (together with the organ of Corti, Fig. 1A) and vestibular end organs from 10-week-old CBA/J mice. Cells isolated from the cochlea include IHCs, OHCs, supporting cells (SCs), spiral ganglion neurons (SGNs), and other accessory cells. Some examples of individual IHCs and OHCs are shown in Fig. 1A. Cells isolated from vestibular sensory epithelia include type I HCs, type II HCs, SCs, vestibular neurons and accessory cells. Type II HCs and SCs express SOX2 (Fig. 1B). Thus, *Sox2*/SOX2 is a marker for these cell types in the vestibular sensory epithelia (Jan et al., 2021; Wilkerson et al., 2021). Some

representative images of type I and type II HCs isolated from maculae of utricle and saccule as well as from crista ampullaris are presented in Fig. 1C.

To comprehensively assess the molecular profiles of inner ear HCs, we conducted scRNA-seq using the cells isolated from the auditory and vestibular sensory epithelia. The cellular diversity in the cochlear and vestibular sensory epithelia was assessed by a t-distributed Stochastic Neighbor Embedding (t-SNE) analysis followed by cluster annotations based on the expression of known marker genes (Fig. 1D,E) (Burns et al., 2015; Jan et al., 2021; Ranum et al., 2019; Wilkerson et al., 2021). Upon cluster annotation, HC types were separated for the downstream analysis by assessing their generic and unique marker genes (Fig. 1F). For HC type, we aggregated the number of reads for each gene across all single cells to generate pseudo-bulk expression profiles (Table S1). Based on the expression of 26 core genes (Fig. 1G), 1,522 individual cells were identified as HCs, including 131 IHCs, 668 OHCs, 588 type I HCs, and 135 type II HCs for our downstream analysis.

1. Similarities among HC types

We utilized the pseudo-bulk and single-cell gene expression profiles to compare the four HC types. Transcriptomes of adult IHCs and OHCs have been compared extensively in the past (Li et al., 2018; Ranum et al., 2019). Thus, we focused our analyses on the differences between cochlear and vestibular HCs, as well as between type I and type II HCs. Principal component analysis (PCA) was used to denote variance across the four types of HCs. The first principal component (PC1) shows that the largest differences are between cochlear and vestibular HCs (Fig. 2A). The distribution across PC2 indicates that the similarity between type I and type II HCs is greater than the similarity between IHCs and OHCs, suggesting more homogeneity among type I and type II HCs. Gene expression profiles of single HCs were also used to analyze similarities among four different HC types (Fig. 2B). Despite heterogeneity of individual HCs in each type, three-dimensional PCA visualization of single cells draws similar conclusions to the pseudo-bulk PCA, suggesting higher transcriptomic similarity between vestibular HCs in contrast to cochlear HCs. Interestingly, PCA analysis also shows that IHCs share a greater transcriptomic similarity with type II HCs than with type I HCs when vestibular and cochlear HCs are compared (Fig. 2A, B).

2. Differentially expressed genes in HC types

Next, we examined the number of genes that are shared and unique among four types of HCs based on pseudo-bulk expression profiles. Figs. 2C and D show the genes shared among two or more HC types, as well as those uniquely expressed by a single HC type. Approximately 71% of the detected genes are shared among all four HC types.

Although HCs share 71% of genes, the smaller proportion of genes unique in each HC population may underlie their specific biological identities. We performed a pairwise differentially expressed gene (DEG) analysis between HC types (Fig. 2E). We defined our DEGs as those with an expression level above 0 and a minimum of 2-fold change (log2 ≥ 1) between the two cell populations with statistical significance of $p \leq 0.01$.

Comparison of IHCs and OHCs revealed the increase expression of 154 and 123 DEGs in IHCs and OHCs, respectively. This analysis revealed previously characterized DEGs in IHCs (e.g., *Otof, Slc17a8*) and OHCs (e.g., *Ocm, Slc26a5, Chrna10*) as well as genes whose functions are not yet to be characterized, including *Atp2a3, Calb2, Dnajc5b, Ripor3* and *Scd1* in IHCs, and *Aqp11, Dnm3,* and *Sh3gl3* in OHCs.

Comparison between IHCs and type I HCs identified 174 DEGs in IHCs and 265 DEGs in type I HCs. Previously uncharacterized DEGs enriched in type I HCs such as *Adam11, Car12, Lpgat1, Spp1* and *Pcdh20* are related to cell-matrix interactions, mineralized matrix, calcification, and acid-base balance.

When IHCs are compared to type II HCs, 155 and 228 DEGs are found in IHCs and type II

HCs, respectively. DEGs enriched in type II HCs include *Ccer2, Cib3, Cxcl14, Fbxo32, Ldhb, Nrxn3, Pcdh20* and *Spp1*. These genes play a role in the secretion of extracellular matrix protein, cell adhesion, phosphorylation-dependent ubiquitination, metabolism, and processes related to immunoregulation and inflammation.

When OHCs are compared to type I HCs, 180 and 289 DEGs are found in OHCs and type I HCs, respectively. *Adam11, Car12, Cib3, Lpgat1, Pcdh20* and *Spp1* are highly enriched in type I HCs. Furthermore, the comparison between OHCs and type II HCs identified 197 DEGs in OHCs and 317 DEGs in type II HCs. While most DEGs overlapped with those identified in the IHC and type II HC comparison, this analysis revealed additional type II HC DEGs such as *Evl, Gsn, Fam183b, Mrps6*, and *Nrxn3*. Comparison of type I and type II HCs revealed the enrichment of 35 DEGs in type I HCs and 59 DEGs in type II HCs. Newly identified markers for type II HCs include *Dlk2, Dtna, Fbxo32, Otog, Pcp4, Ptn, Sparc, Sparcl1, Tctex1,* and *Tmod1* whereas the top DEGs in type I HCs included *Adam11, Atp2b2, Bdnf, Bmp2, Cacna2d4, Car12, Kcnab1, Lpgat1* and *Spp1.*

Since the molecular properties of vestibular HCs are less known compared to cochlear HCs, we performed a gene ontology (GO) and overrepresentation analysis to examine biological processes enriched in vestibular HCs compared to cochlear HCs. The comparison of processes enriched in vestibular HCs revealed GO terms related to cilium organization and microtubule-based cilium motility (Fig. 2F). We also compared the biological processes enriched in type I and type II HCs. This comparison revealed the enrichment of processes related to oxidative phosphorylation, proton transmembrane transport, aerobic and cellular respiration in type I HCs (Fig. 2G), while the enriched processes in type II HCs are related to p53-mediated signal transduction and actin filament depolymerization and regulation (Fig. 2H).

3. Marker genes for different HC types

Previous studies have characterized some marker genes in different HC types. We assessed the expression of both previously characterized and newly identified HC genes across all four HC types (Fig. 3A). Genes shared among all four HC types such as *Cib2, Tmc1,* and *Espn* are demonstrated in the top rows. We also identified genes not known to be expressed in all HC types. An example is *Tjap1,* which encodes a tight junction-associated protein. Certain genes are highly expressed in one HC type while weakly expressed in the other. *Cdh23, Rorb* and *Osbp2* are highly expressed in cochlear HCs than in vestibular HCs whereas, genes such as *Ldhb, Fbxo32, and Gsn* are highly expressed in vestibular HCs but only weakly expressed in cochlear HCs. We identified several genes that are only expressed in vestibular HCs but not in cochlear HCs such as *Cfap43, Cfap44, Cfap126, Cib3, Cxcl14, Kcnb1, Kif3, Lpgat1, Mlf1, Pcdh20, Pifo, Slc9a3r2, Slco3a1, Tmc2* and *Sppl1,* which could potentially be used as markers for vestibular HCs. Moreover, *Adam11, Cacna2d4, Car12,* and *Shank2* are found to be only expressed in type I HCs, while *Ccer2, Cfap45, Dlk2,* and *Rprm* are only expressed in type II HCs. Our analysis also revealed new marker genes for IHCs (*Atp2a3, Rims2, Ripor3*) and OHCs (*Aqp11, Mmd* and *Sh3gl3*). *Cfap43, Cfap44, Cfap45, Cfap126, Kif3, Mlf1* and *Pifo* are all associated with kinocilium structure and function.

We utilized single molecular fluorescent *in situ* hybridization (smFISH) and immunostaining techniques to validate the expression of 12 genes in HCs (Fig. 3B,C). The expression patterns of these genes and proteins were highly consistent with our observations from scRNA-seq analysis. Overall, our results identified novel marker genes and previously unidentified expression patterns among the four HC types.

4. Genes related to HC specialization in different HC types

Next, we focused our analysis on evaluating the genes associated with HC function. We compared the expression of 208 genes related to HC specialization, including stereocilia and

apparatus for mechanotransduction, ion channels, and synapses (Fig. 4A). Among the 112 of many genes associated with stereocilia and mechanotransduction apparatus (Shin et al., 2013), *Calm1, Calm2, Eps8, Espn, Fbxo2, Dynll2, Ush1c, Ywhae, Tmc1, Tmie, Cdh23, Pcdh15, Ank1, Ank3,* and *Lhfpl5* were highly expressed in all four HC populations. Others were highly expressed in only one or two HC populations. *Atp2a3, Calb2,* and *Dpysl2* were highly expressed in IHCs, while *Lmo7, Ocm,* and *Strc* were highly expressed in OHCs. Moreover, expression of *Dpysl2, Cdh23,* and *Cib2* was higher in cochlear HCs than in vestibular HCs, while *Xirp2, Pls1, Slc9a3r2,* and *Tubb4b* were more highly expressed in vestibular HCs than in cochlear HCs. Moreover, some genes were uniquely expressed in either cochlear or vestibular HCs. For example, *Cib3* and *Tmc2* are expressed in vestibular HCs but not in cochlear HCs.

All HCs possess ion channels. Several genes related to stretch-activated ion channels, such as *Trpc1* and *Trpm4,* were detected. Genes for Cl^- and Na^+ channels were expressed. For Ca^{2+} and K^+ channels, *Cacna1d and Kcna10* were expressed in all four HC types with varying levels of expression. In cochlear HCs, *Cacna1d, Kcna10, Kcnab1, Kcnj16 and Kcnma1* were expressed in IHCs, whereas *Cacna1d, Kcna10, Kcnk1, Kcnma1, Kcnn2* and *Kcnq4* were expressed in OHCs. In the vestibular HCs, *Cacna2d4, Kcna10, Kcnab1,* and *Kcnma1* showed relatively high expression in type I HCs whereas type II HCs indicated a relatively high expression of *Cacna2d4, Cacng5, Kcna10, Kcnb1, Kcnh2,* and *Kcnh7*. *Best1, Clic, Hcn1,* and *Kcnh7* were only expressed in vestibular HCs.

Next, we examined the genes related to synapses (Fig. 4A). Our results indicated expression of *Ctpb2, Dlg1*, *Homer2, Otof, Pclo*, and *Snap91* expression in all HCs with varying degree. A higher expression of *Dnm1, Otof, Rims2, Slc17a8, Snap91,* and *Stx7* was seen in IHCs while *Dlg1, Dnm3*, *Snap9, Chrna9,* and *Chrna10* showed higher expression in OHCs. Some of the highly expressed genes in type I HCs include *Dnm1, Kif3a, Pclo, Shank2, Slc17a8, Syt13, Syt14, Chrna9,* and *Chrna10,* whereas type II HCs showed relatively higher expression of *Kif3a, Otof, Shank2, Stx7,* and *Syt13*. We employed smFISH to validate the expression of 8 additional genes across the four HC types. The expression patterns shown in Fig. 4B are highly consistent with our analysis.

5. Gene signatures of primary cilia in cochlear and vestibular HCs

Since our analysis revealed an enrichment of cilium-related GO terms (Fig. 2F) and axonemal genes such as *Cfap43, Cfap44, Cfap45, Cfap126, Kif3, Plf1,* and *Tubb4b* (Fig. 3A) in vestibular HCs, we sought to investigate the composition and nature of the kinocilium (Fig. 5A). Proteomics-based approaches have contributed to the development of cilia-associated protein databases. We utilized several well-established databases, including CiliaCarta (Dam et al., 2019), the SYSCILIA gold standard (SCGSv2) (Vasquez et al., 2021), and CilioGenics (Pir et al., 2024) to compile a list of cilia-related genes. Collectively, these databases include ~1,000 genes/proteins. We noted a significant overlap of cilia-related genes from these databases with our transcriptome (Fig. 5B). GO analysis of the overlapping genes revealed enrichment in cellular localization and biological processes primarily related to cilia organization, assembly, maintenance, intracellular transport, and microtubule dynamics particularly associated with motile cilia. Additionally, molecular function analysis highlights associations with motor activity, BBSome binding, and dynein chain binding (Fig. S1).

Primary cilium is a sensory organelle that responds to and transmits the external signal to the cell's interior. Structurally, primary cilia are characterized by the presence of nine microtubule doublets (MTDs) encircling the shaft, which transition into a disorganized structure distally (Fig. 5C). Since kinocilia have been considered as primary cilia, we first examined the expression of primary cilia-related genes in vestibular and cochlear HCs. Among approximately 420 primary cilia-related genes/proteins (Dam et al., 2019; Pir et al., 2024; Vasquez et al., 2021), we detected

the expression of 410 genes in at least one type of HCs. Fig. 5D shows the top 50 abundantly expressed primary cilia-related genes in type II HCs compared to the other three HC types. Most of these genes were detected in all four HC types except a few genes, such as *Mlf1, Ttc21a,* and *Tmem218* that were weakly or not expressed in cochlear HCs. Primary cilia are enriched in receptors and effectors for key pathways, including GPCR, cAMP, Ca^{2+}, RTK, TGF-beta, MAPK, TOR, BMP, Wnt, Notch, and Rho signaling (Anvarian et al., 2019), localized to the ciliary shaft, transition zone, and BBSome (Hansen et al., 2024). We analyzed the expression of these genes in HCs and found a higher level of expression of these pathway-related genes in vestibular HCs than in cochlear HCs (Fig. S2).

Intraflagellar transport (IFT) involves anterograde and retrograde transport of molecules along the axoneme of cilia, facilitating the transport of components between the ciliary base and tip (Ma et al., 2023). IFT is essential for the proper assembly and maintenance of both primary and motile cilia. Thus, we assessed the expression of IFT-associated genes in HCs. Most of the genes are enriched in vestibular HCs compared to cochlear HCs (Fig. 5D). Immunostaining confirmed the expression of IFT172 and CLUAP1 in the kinocilia of vestibular HCs (Fig. 5E).

6. Gene signatures of motile cilia in vestibular HCs

Motile cilia are highly conserved organelles across different organisms and tissues, though they exhibit organism- and tissue-specific adaptations (Leung et al., 2025). Recent advances using proteomics of isolated motile cilia from various ciliated tissues have enabled the profiling of genes associated with motile cilia. To explore whether the kinocilium possesses a molecular composition characteristic of motile cilia, we compared our HC transcriptomes with multi-tissue proteomics datasets derived from different organisms, including human, bovine, porcine, and murine, as well as diverse motile ciliary tissues such as sperm, oviduct, ventricle, and trachea (Leung et al., 2025) (Fig. S3). Our analysis revealed a significant overlap, particularly among axonemal components of motile cilia, with strong enrichment in vestibular HCs compared to cochlear HCs. The axoneme of motile cilia and flagella is a cylindrical structure harboring a canonical “9+2” arrangement, where nine microtubule doublets surround two microtubule singlets in the center (Fig. 5C). Altogether, the axoneme machinery consists of nine doublet microtubules (DMTs), two rows of inner and outer dynein arms (IDAs and ODAs), nexin-dynein regulatory complex (N-DRC), two singlet central pair complex (CPC), three radial spokes (RSs), microtubule inner proteins (MIPs), and external coiled-coil regions. The motility unit is arranged in a 96-nm repeat module along the CPC. Recent cryo-EM and cryo-electron tomography (cryo-ET) studies have provided a more comprehensive identification of this module repeat(Chen et al., 2023; Leung et al., 2025; Walton et al., 2023). To understand the molecular composition and function of kinocilia, we focused our analysis on the expression of genes associated with the structure of motile cilia. First, we aggregated the genes related to each component of the motile cilia structure and assessed the expression of these genes among the HC types. We noted a robust expression of motile cilium-related gene signatures in vestibular HCs, while cochlear HCs expressed little to none (Fig. 5F). Next, we further assessed the expression of the key genes related to motile cilia machinery (Fig. 5G), including the 96-nm module and CPC, based on the current known localization from biochemistry and proteomics.

The 96-nm axonemal repeat of mammalian epithelial cilia contains proteins encoded by 128 genes[24]. We found that 112 of 128 genes related to axonemal repeat were expressed in adult vestibular HCs, while only ~15% of those were detected in cochlear HCs. Genes encoding axonemal dynein (IDAs and ODAs), such as *Dnah5* and *Dnah6*, as well as radial spoke components (*Wdr66, Cfap206, Cfap61, Iqub*), N-DRC components (*Drc1, Iqca*), and MIPs (*Cfap126, Wdr63*) were predominantly expressed in vestibular HCs with little to no expression in cochlear HCs (Fig. 5G). Axonemal CCDC39 and CCDC40, which form external coiled-coil regions,

are the molecular rulers that organize the axonemal structure in the 96-nm repeating interactome and are required for the assembly of IDAs and N-DRC for ciliary motility (Becker-Heck et al., 2011; Merveille et al., 2011; Oda et al., 2014). Our results indicate a high expression of *Ccdc39* and *Ccdc40* in vestibular HCs, whereas little to no expression was observed in cochlear HCs.

RFX and FOXJ1 transcription factor families are key regulators of ciliome gene activation, with RFX controlling genes in both motile and non-motile cilia, while FOXJ1 specifically governs motile cilia formation (Choksi et al., 2014). Our data indicated that *Foxj1* was moderately expressed in vestibular HCs but only weakly expressed in cochlear HCs (Fig. 5G). Other genes that regulate motile cilia formation, including *Lrrc6,* were also expressed at high to moderate levels in vestibular HCs compared to cochlear HCs. We also found a strong enrichment of transcriptional targets associated with vestibular HCs, particularly those involved in motile cilia programming and maintenance. Thus, the expression of these transcription factors including *Foxj1* may suggest that their expression is necessary for the maintenance of kinocilia in adult vestibular HCs.

Next, we examined whether the expression of these genes is conserved in vestibular HCs across different species. Using published datasets (Barta et al., 2018; Wang et al., 2024), we obtained the orthologs of axoneme-related genes in adult zebrafish inner ear HCs and human vestibular HCs. Fig. 6A shows the expression of these genes in adult mouse, zebrafish, and human vestibular HCs. While the expression level varies, the majority of these genes are expressed across species. The exceptions are *Dnah3* and *Dnah12*, which are expressed in zebrafish HCs but not in mammalian vestibular HCs.

We conducted immunostaining and high-resolution confocal imaging to validate the expression of key motile cilium markers in the kinocilia. As indicated in Fig. 6B, FOXJ1 is expressed in the nucleus of vestibular HCs, while CCDC39, CCDC40, TEKT1, DNAH5, and DNAH6 are expressed in the kinocilia. Collectively, our findings provide evidence corroborating the presence of motile cilium machinery in the kinocilia of vestibular HCs.

Furthermore, since nascent cochlear HCs possess kinocilia (Fig. 6C), we investigated whether cochlear HCs express motile cilium-related genes by utilizing publicly available P2 cochlear and vestibular HC transcriptomes (Burns et al., 2015). Assessment of expression of genes related to motile cilia machinery in the nascent vestibular and cochlear HCs revealed a less drastic difference between neonatal cochlear and vestibular HCs than observed between adult HCs (Fig. 6D). However, we did note the absence of some key genes such as *Dnah6, Dnah5,* and *Wdr66* in P2 cochlea. Immunostaining confirmed the lack of expression of CCDC39, CCDC40, and DNAH6 in neonatal cochlear HCs at the protein level while they were expressed in kinocilia of vestibular HCs at P2 (Fig. 6E). Thus, our data shows that the molecular composition of kinocilia is different between neonatal cochlear and vestibular HCs and that the kinocilium of neonatal cochlear HCs does not possess signatures of motile cilia.

7. Vestibular kinocilia exhibit a hybrid morphology with features of both primary and motile cilia.

TEM studies have characterized the ultrastructure of kinocilia across species, revealing evidence of complex and regionally specialized organization (Kikuchi et al., 1989; Nagel et al., 2014; O'Donnell and Zheng, 2022). Archival TEM images from Kachar's lab, including longitudinal sections of frog vestibular hair bundles (Fig. 7A), highlight a distinct zonal architecture along the kinocilium axis. At the distal tip, a prominent kinociliary bulb is observed, while the base anchors the axoneme within the cuticular plate. Two pairs of microtubule doublets span the full length of the kinocilium. The central pair of singlet microtubules, typical of motile cilia, is maintained throughout most of the shaft but disappears in the distal and transitional zones. This configuration results in a dynamic shift from a canonical 9+2 arrangement centrally to a 9+0 pattern at both the base and tip. These observations underscore the heterogeneous and hybrid nature of vestibular

kinocilia, integrating structural features of both primary and motile cilia. Such duality likely supports their unique functional role at the intersection of mechanosensation and signal transduction.

8. Evidence that vestibular kinocilia can exhibit motility

Although vestibular kinocilia are traditionally regarded as non-motile—lacking the rhythmic beating characteristic of respiratory cilia—they are known to play key structural and developmental roles. These include establishing hair bundle orientation and contributing to mechanosensory polarity during inner ear development. However, archival imaging data from our laboratory using acute preparations of bullfrog semicircular canal sensory epithelia (cristae) reveal direct evidence of spontaneous kinociliary motility in a subset of HCs (Fig. 7B; Videos S1 and S2). This motility exhibited the characteristic flagella/cilia beating pattern and occurred at a frequency of approximately 10 Hz. The observed displacements were sufficiently large to induce movement of the entire hair bundle, indicating it can generate forces to influence hair bundle dynamics. Interestingly, this phenomenon was detected in only ~5% of saccular HCs, likely due to variable preservation of HC and kinociliary integrity in vitro. These findings suggest that while motility is not ubiquitous, vestibular kinocilia are capable of active movement under specific physiological conditions, challenging the strict classification of these structures as non-motile.

Next, we explored whether the kinocilia of vestibular HCs from adult mice are motile by utilizing the photodiode technique to detect bundle motion(Jia and He, 2005). This technique can detect motion in the 10-nm range after averaging for synchronized signals. Since spontaneous motions are not synchronized and cannot be averaged to improve signal-to-noise ratio, we captured the responses in the time domain and averaged them in the frequency domain after a fast Fourier transform. This allows us to detect unsynchronized cilia motion even if the signal is close to the noise level at the time domain. We first used the cilia in the epithelial lining of the Eustachian tube, which is an extension of airway epithelia, as a positive control for motility measurement. Fig. 7C shows an image of airway cilia using differential interference contrast optics. We measured motion of the top segment of cilia (black frame in Fig. 7C). Fig. 7D shows two representative waveforms of airway cilia beat with a magnitude between 700 and 1500 nm. The two responses shown in Fig. 7D have main frequency components at 6 to 9 Hz. Next, we measured the movement of the top segment of the hair bundle from the mouse crista ampullaris (Fig. 7E). Since the kinocilium is tightly attached to the stereocilia bundle, we measured the whole bundle's motion due to the difficulty of taking measurements from a single kinocilium. The waveform (black trace in Fig. 7F) was obtained from crista HCs bathed in perilymph-like solution (L-15 medium) with 2 mM of Ca^{2+}. When the motion was analyzed in the frequency domain, the peak at ~7 Hz was evident (Fig. 7F). To rule out the possibility that the bundle motion is driven by the mechanotransduction-related activity (Benser et al., 1996; Martin et al., 2003), we treated the crista ampullaris in Ca^{2+}-free medium with EGTA for 2 minutes to break the tip-link(Jia et al., 2007; Ricci et al., 2003). We then replaced the Ca^{2+}-free medium with normal L-15 medium. Spontaneous bundle motion was still detected (two red traces in Fig. 7F), suggesting that the motion is independent of the transduction channel activity. We measured spontaneous bundle motions from 52 crista HCs from six mice. Spontaneous motion was only detected in eight HCs while the majority of HCs did not display detectable bundle motion. An example of a lack of response is also shown (blue trace in Fig. 7F). Interestingly, we noted that the hair bundle motion was substantially smaller than that of airway cilia (Fig. 7D) and bullfrog saccular HCs.

9. Predicted model of the 96-nm modular repeat in adult vestibular kinocilia

Next, we sought to understand why kinocilium motility in mouse vestibular HCs was substantially smaller than that of bullfrog saccular HCs and airway cilia. The difference in magnitude may reflect the structural variance of the microtubule-associated motor protein

complex in kinocilia. Recent developments in cryo-EM and artificial intelligence (AI)-enabled structure prediction have led to the highly conserved atomic structural model of the 96-nm modular repeats of axonemes (Chen et al., 2023; Leung et al., 2025; Walton et al., 2023). We applied our single-cell-based axonemal gene dataset to this model to construct a predicted molecular architecture of the highly conserved 96-nm repeat in vestibular kinocilia using information from human respiratory doublet microtubule and associated axonemal complexes. In vestibular HCs, we found expression of all 18 genes associated with the ODA and their docking complexes, all 11 N-DRC genes, and all 7 microtubule-associated proteins (MAPs), along with 36 out of 37 radial spoke genes and 19 out of 23 IDA-related genes. Additionally, 20 of the 31 genes encoding MIPs, which stabilize microtubule doublets, were also expressed. The structural integration of these gene products into the 96-nm axonemal repeat is visualized in Fig. 8. Based on our predicted model, the absence of *Dnah3* and *Dnah12*, along with *Acta2* and *Cfap100*, would result in the loss of specific single-headed IDA components (highlighted in gold). Although 4 out of the 23 IDA-related genes were not expressed, the overall IDA structure appears reduced rather than entirely absent, as DNAH6 remains localized in vestibular kinocilia (Fig. 6B). Additionally, the lack of expression of 11 other genes is associated with a reduction in MIPs (marked in pink) compared to motile cilia. Unlike other axonemal components, MIPs exhibit a greater variability across species. The missing genes in our HC datasets and their roles in axonemal complex, cilium motility and ciliopathy are listed in Fig. 8B. Based on our predicted model, we speculate that lack of expression of DNAH3 and DNAH12 may affect the motility of kinocilia of vestibular HCs, resulting in smaller motions than that of motile cilia.

DISCUSSION

This is the first study to compare transcriptomes among four types of HCs from adult mouse inner ear. We observed several differences in gene signatures related to HC specialization, which may underlie distinct properties of mechanotransduction, membrane conductance, and synaptic transmission seen among four different HC types. Differential expression also explains why loss of function of a gene such as *Tmc1, Cib2,* or *Cib3* leads to differential auditory and vestibular phenotypes in mouse models and humans. Our dataset is expected to serve not only as a highly valuable resource for unraveling the molecular mechanisms of the biological properties of HCs but also for assisting the auditory and vestibular research community in identifying and exploring the functions of disease-related genes.

Since biological processes enriched in vestibular HCs are related to cilia and cilium motility, we focused our analyses on kinocilia. Kinocilia have long been regarded as primary cilia. However, the molecular properties of kinocilia are largely unexplored. Our study suggests that kinocilia serve dual roles as both primary and motile cilia. Primary cilia are a major hub in receiving and transmitting signals from the environment. A recent study has demonstrated the expression of proteins related to transduction pathways and receptors in primary cilia using spatial proteomics (Hansen et al., 2024). We showed that vestibular and cochlear HCs expressed genes encoding proteins for signal transduction pathways and receptors. Although the localization of those proteins in HC kinocilia needs further validation, our analysis highlights the expression of diverse primary cilia signaling genes shared among different HC types, emphasizing their conserved and potentially specialized roles in cellular signaling and ciliary function.

The tip of motile cilia is a region with specialized proteins (Legal et al., 2023). In multi-ciliated cells, CCDC33 and CCDC78 are found at the very end of the cilium and help organize other proteins like SPEF1, CEP104, and EB3/MAPRE3 (Hong et al., 2025; Legal et al., 2024, 2023). We found expression of all the genes encoding these proteins except *Ccdc78*. Although we did not study the tip of the kinocilium, its bulb shape suggests it may also contain specialized proteins. In bullfrog HCs, the kinocilial bulb binds to the overlaying otoconial membrane (Jaeger et al., 1994;

Kachar et al., 1990) and shows strong labeling for β-tubulin and cadherin 23 (Jaeger et al., 1994; Kachar et al., 1990; Lagziel et al., 2005), and a recent study showed that *saxo2* overexpression causes bulbed zebrafish kinocilia with Saxo2 accumulating at the tip (Erickson et al., 2023). These bulbed tips may reflect specialized regulation of ciliary cap proteins(Legal et al., 2023) that help organize or stabilize the plus ends of axonemal microtubules—an area that remains to be explored in kinocilia.

The most important and novel findings of our study are that adult vestibular HCs express genes related to the 96-nm axonemal repeat complex, a hallmark structural component of motile cilia. Orthologous axonemal-related genes are identified in zebrafish and human vestibular HCs, underscoring the evolutionarily conservation of the molecular composition of the complex in vestibular HCs across vertebrates. Furthermore, we observed robust spontaneous kinocilia motility in bullfrog saccular HCs and small spontaneous bundle motion in mouse crista HCs. The oscillation frequency is ~10 Hz at room temperature, in line with an ATP-mediated mechanism. The pattern of movement is similar to that seen in motile cilia and flagella. Importantly, the power stroke of a single kinocilium is sufficient to drive oscillation of the hair bundle. Early studies reported observation of spontaneous flagella-like oscillations of kinocilia in vestibular HCs in frogs and eels (Flock et al., 1977; Rüsch and Thurm, 1990), as well as in zebrafish HCs in the early otic vesicle (Stooke-Vaughan et al., 2012; Wu et al., 2011) (see Movie 8 ref 48). In our study, we observed kinociliary motility in only a subset of the cells. There are two primary reasons why such motility has not been consistently observed in both current and previous investigations. First, HCs in vitro rapidly lose their physiological integrity when removed from their native electrochemical environment. This is especially critical for mammalian HCs, which depolarize quickly once this environment is disrupted. Second, the process of acute tissue dissection and handling may compromise the integrity of the kinociliary membrane, which—under native conditions—is tethered to the overlying extracellular matrix. Such disruptions may impair kinocilia integrity and the metabolic conditions (such as depletion of ATP) essential for sustaining ciliary motility.

Although we observed kinocilium-driven bundle movement in adult mouse vestibular HCs, the magnitude of motility was not as large as that seen in bullfrog HCs and other motile cilia. Single-cell transcriptomic analysis showed that 16 genes associated with the 96-nm repeat axonemal core were not detected in our mouse HC transcriptome datasets. Although 11 genes related to MIPs were not detected, MIPs are the most heterogeneous components across different types of cilia, such as sperm and airway cilia (Leung et al., 2025; Tai et al., 2023). Thus, we do not expect a lack of expression of these 11 genes would have a substantial impact on kinocilia motility, although loss of function of *Pierce1* and *Pierce2* leads to defeat on cilia motility and laterality in zebrafish (Gui et al., 2021; Sung et al., 2016). However, the lack of expression of two genes associated with IDAs (*Dnah12*, *Dnah3*) may lead to the loss of specific single-headed IDA components. Mutations of *DNAH3* and *DNAH12* are linked to male infertility and dynein dysfunction in humans (Meng et al., 2024; Yang et al., 2024). Moreover, it has been shown that mutations of DNAH12 cause male infertility by impairing DNAH1 and DNALI1 recruitment. However, it does not affect the tracheal tract and oviductal cilia organization (Yang et al., 2024). For other two IDA-related genes (*Acta2, Ccdc37*) and one RS-related gene (*Morn3*), no ciliopathy has been linked to mutations of these three genes so far. We speculate that lack of expression of DNAH3 and DNAH12 contributes to smaller kinocilia motility in mammalian vestibular HCs. Since *dnah3, dnah12, acta2*, and *cfap100* are all expressed in zebrafish HCs (Giffen et al., 2024), kinocilia motility of zebrafish HCs and presumably bullfrog HCs is expected to be greater than that of mouse vestibular HCs. The difference in magnitude of kinocilia motility observed from bullfrog and mouse vestibular HCs is consistent with our predicted model.

Recent study shows that while the 96-nm repeat structure of motile cilia in multi-ciliated epithelia and sperm flagella is similar at the core (Chen et al., 2023; Leung et al., 2025; Walton et al., 2023), sperm DMTs exhibit added complexity through ~30 unique proteins not found in epithelial cilia (Chen et al., 2023). These specializations reflect the unique demands of sperm motility, including greater length, a distinct waveform, and stiffening accessory structures. In contrast, epithelial DMTs are structurally conserved across motile tissues (Leung et al., 2025), reflecting the shared architecture of epithelial cilia—typically 5–10 μm long with similar waveform behavior. This uniformity is notable given the diverse fluid environments and varying sensitivities to ciliopathic mutations. Our analysis indicates that the kinocilium, despite its exceptional length (60–70 μm) and mono-ciliated nature, does not exhibit the molecular specializations observed in sperm at the axonemal core. Instead, its gene expression profile closely resembles that of multi-ciliated epithelial cilia, highlighting its unique identity as a structurally extended but molecularly conventional motile cilium within the sensory epithelium.

Spontaneous oscillation and active hair bundle motion of turtle and frog HCs were reported before (Benser et al., 1996; Crawford and Fettiplace, 1985; Denk and Webb, 1992; Howard and Hudspeth, 1987; Martin et al., 2003). However, the active motion is thought to arise from the interplay of the hair bundle's negative stiffness with the activity of adaptation motors and the Ca^{2+}-dependent relaxation of gating springs (Martin et al., 2003). The kinocilium motility we observed in bullfrog vestibular HCs is clearly not driven by mechanisms associated with mechanotransduction apparatus, as we saw an active flagellar-like movement in the individual kinocilium itself. More importantly, spontaneous motion was not affected by breaking the tip links. Although we were unable to determine the identity of HCs that exhibited kinocilium motility, type I and type II HCs have the molecular machinery for motility since the genes related to motile cilia were detected in both types of vestibular HCs.

In addition to anchoring the hair bundle to the overlying extracellular matrix, the kinocilium is ideally positioned to modulate mechanical stimuli transmitted to the mechanosensitive stereocilia. The spontaneous motion observed in this study is likely a byproduct of intrinsic force generation, as well as a putative form of regulated motility. This activity may serve to dynamically modulate tip-link tension, thereby influencing the mechanosensitivity of vestibular HCs (Roberts et al., 1988). Such a mechanism is likely conserved among kinocilium-bearing vestibular HCs across both non-mammalian and mammalian species. By contrast, in the mammalian cochlea, this mode of active modulation has been supplanted by the somatic motility of OHCs (Brownell et al., 1985; Dallos et al., 2008; Kachar et al., 1986; Liberman et al., 2002; Zheng et al., 2000).

In summary, this study is the first to demonstrate that the kinocilium of vestibular HCs is a unique hybrid cilium, exhibiting near-complete molecular features of both primary and motile cilia. While it shares structural and molecular similarities with motile cilia and sperm flagella, it also possesses distinct architectural and functional characteristics. We also provide a molecular model of the 96-nm axonemal repeat. Future investigations employing vestibular kinocilium-specific proteomics, cryo-ET, and single-particle analysis will be critical for fully characterizing kinocilium molecular composition and organization. Although kinocilium motility was observed in both bullfrog saccular and mouse vestibular HCs, the mechanisms by which this motility influences HC mechanosensitivity or other biological properties of the vestibular sensory epithelium remain to be elucidated.

MATERIALS AND METHODS

Male and female CBA/J mice were purchased from the Jackson Laboratory (Stock #:000656) and reared in Animal Care Facility of Creighton University and NIDCD. American bullfrogs (*Rana catesbiana*) were purchased from Carolina Biological Supply Co. The animal usage and care were approved by the Institutional Animal Care and Use Committees of Creighton University (Protocol

#1046.3) and NIDCD (NIDCD ACUC Protocol #1215).

1. Cell dissociation, cDNA libraries preparation and RNA-Sequencing

Male and female CBA/J mice aged 10 weeks were used for scRNA-seq. The cochlear and vestibular end organs (utricle, saccule, and crista) were dissected from the inner ear and placed in Petri dishes containing cold L-15 medium (Gibco; #11320033). After the cochlear and vestibular sensory epithelium and neurons were dissected out, they were separately transferred into two individual 1.5 ml tubes for enzymatic digestion (Collagenase IV from Sigma, concentration: 1mg/ml collagenase) in L-15 medium. After 10 minutes of incubation at room temperature, the enzymatic solution was removed and replaced with 400 µl L-15 media containing 10% fetal bovine serum. The tissues in two tubes were mechanically triturated by 200 µL Eppendorf pipette tips. After that, the suspension containing cochlear and vestibular cells was then passed through 40 µm strainers for filtration and pelleted at 300 g for 5 mins. After removing extra media, cells were then reconstituted in the 50 ul L-15 with 10% fetal bovine serum media and used for cDNA library preparation. Seven mice were used for each biological replicate. Six biological replicates for cochlear sensory epithelium and four biological replicates for vestibular sensory epithelia were prepared for scRNA-seq.

The emulsion droplets were constructed using a 10x Genomics Controller device following the manufacturer's instruction manual. cDNA libraries were constructed using the 10x Genomics Chromium Single Cell 3' Reagent Kits V3.1. High Sensitivity DNA Kits (Agilent Technologies) were used to perform the quality control for each library in an Agilent 2100 Bioanalyzer. cDNA libraries were sequenced in an Illumina NextSeq 6000 sequencer aiming for 240 billion 150 bp long paired-end reads.

2.Single-cell RNA-seq data process and analysis

Raw transcriptomic datasets of adult cochlear and vestibular HCs from scRNA-seq have been deposited to GEO (GSE283534). The FASTQ files were mapped to mm10 reference genome to generate the single-cell expression matrices following the CellRanger count pipeline (version 6.1.2). The Cellranger output data was then processed with the Seurat package (version 4.3.0) in R (version 4.1.3).

Genes expressed in at least ten cells were included in the analysis. Cells with numbers of expressed genes <200 or >3,000 and cells with numbers of unique molecular identifiers (UMI) > 15,000 were filtered out. Cells with >20% mitochondrial genes were also excluded from the analysis.

The gene expression data from individual samples were converted into a natural logarithm and normalized under the same condition. Data from six cochlear and four vestibular replicates were integrated separately based on the anchors identified from the top 2,000 highly variable genes of individual normalized expression matrices. The Shared Nearest Neighbor graph method can calculate the neighborhood overlap (Jaccard index) between every cell and its nearest neighbors, which was used for the cluster determination at a resolution of 0.6 on PCA-reduced expression data for the top 30 principal components.

Clustering results for cochlear and vestibular datasets were visualized separately using t-distributed stochastic neighbor embedding (t-SNE). Cluster annotations were primarily produced using SingleR and then corrected based on the differentially expressed genes (DEGs) for each cluster and the well-known cellular markers for cochlear and vestibular cells.

Entrez Gene, HGNC, OMIM, and Ensembl database were used for verification, reference, and analyses. CiliaCarta (https://ngdc.cncb.ac.cn/databasecommons/database/id/6383), Primary Cilium Proteome Database (https://esbl.nhlbi.nih.gov/Databases/CiliumProteome/), and Ciliogenics (https://ciliogenics.com/) were also used for reference.

GO analysis in Fig. S1 was performed using ShinyGO 0.82(Ge et al., 2020). The Venn

diagrams in Fig. 5B and Fig. S3 were generated using Venny 2.1 (https://bioinfogp.cnb.csic.es/tools/venny/), except for the sperm Venn diagram in Fig. S3E, which was plotted using nVenn (https://bioinfogp.cnb.csic.es/tools/venny/).

3. Immunocytochemistry

The cochleae were fixed overnight with 4% paraformaldehyde at 4^0C. The cochlear and vestibular sensory epithelia were dissected out. After several washes with PBS, the tissue was blocked for 1 hour with 0.25% normal goat serum in PBS containing Triton-X-100 (0.01%) and goat serum (10%). Primary antibodies against DNM1 (AB3458, Abcam), SLC7A14 (HPA045929, Sigma), TJAP1 (NBP1-80902, Novus), FOXJ1 (14-9965-82, ThermoFisher), CCDC39 (HPA035364, Sigma), CCDC40 (PA5-54653, ThermoFisher), DNAH5 (31079-1-AP, ThermoFisher), DNAH6 (HPA036391, Sigma), TEKT1 (HPA044444, Millipore Sigma), CLUAP1 (PA5-83710, Thermo Fisher), IFT172 (28441-1-AP) and acetylated tubulin (T6793, Sigma) were incubated with the tissues for 12 hours at 4°C. After washes with PBS, secondary antibody (1:500) (Alexa fluor molecular probe 488 or 555; Invitrogen) was added and incubated for 2 hours at room temperature. Alexa Fluro™ 405 or 488 phalloidin (A30104 or A12379, Invitrogen) was used to label stereocilia bundles. Tissues were washed with PBS and mounted on glass microscopy slides with antifade solution (5 ml PBS, 5 ml glycerol, 0.1 g n-propylgallate). Images were captured using Nikon TI-2 Spinning Disk or Zeiss LSM 980 Inverted confocal microscope.

4. Single molecule fluorescence in situ hybridization

Single molecule fluorescence *in situ* hybridization was used to validate the expression of 15 genes in 10 µm-thin sections. Samples were prepared in formalin-fixed paraffin embedded tissue. Probes for 18 genes were purchased from ACD. These genes include *Adam11*, (580971), *Aqp11* (803751), *C1ql1* (465081), *Cdh23* (567261-C2), *Chrna10* (818521), *Cib2* (846681), *Cib3* (1105771), *Dnm3* (451841), *Ikzf2* (500001), *Kcnq4* (707481), *Otof* (485678), *Pcdh20* (467491), *Slc7a14* (544781), *Tmc1* (Cat No: 520911-C2) and *Tbx2* (448991-C2). Methods for the RNAscope™ 2.5 HD Assay from Advanced Cell Diagnostics were followed.

5.Electron microscopy

The mouse cochleae were fixed with 4% paraformaldehyde and 2.5% glutaraldehyde in 0.1 M sodium cacodylate buffer (pH 7.4) with 2 mM $CaCl_2$. The bullfrog saccular macula was fixed with 3% paraformaldehyde, 2% glutaraldehyde, 2% tannic acid and 0.5% calcium chloride in 0.1 M sodium cacodylate buffer (pH 6.8) with 0.1 mM $CaCl_2$ (Kachar et al., 1990). The tissues were then post-fixed for 1 hour with 1% OsO_4 in 0.1 M sodium cacodylate buffer and washed. For scanning electron microscopy, the cochleae were dehydrated via an ethanol series, critical point dried from CO_2, and sputter-coated with platinum. The morphology of the HC stereocilia bundle was examined in a FEI Quanta 200 scanning electron microscope and photographed. For TEM, the bullfrog saccular macula was embedded in plastic (Epon 812 Epoxy Resin) after dehydrated via an ethanol series. 70-nm thin sections were cut with a diamond knife and collected on 300-mesh grids. The thin section was post-stained with 3% uranyl acetate for 15 min and 1.5% lead citrate for 3 min. The preparations were examined in an electron microscope (JEOL 100CX) and photographed.

6. Measurements of ciliary motion

Bullfrogs were anesthetized with 20 µg/g of 3-aminobenzoic acid ethyl ester and decapitated. The saccular macula was carefully dissected out under cooled frog's Ringer solution. The otoliths were gently removed with forceps in fresh Ringer solution(Jaeger et al., 1994). The saccular macula was placed under an Olympus upright microscope and kinocilia motility was visualized using DIC and 60x objective and captured with a camera.

The Eustachian tube was dissected out from CBA/J mice and sectioned along its longitudinal length. The preparation was bathed in L-15 medium (Invitrogen), containing 136 mM NaCl, 5.8

mM NaH_2PO_4, 5.4 mM KCl, 1.4 mM $CaCl_2$, 0.9 mM $MgCl_2$, 0.4 mM $MgSO_4$, and 10 mM HEPES-NaOH (pH 7.4, 300 mmol/l) in an experimental chamber mounted on the stage of a Leica upright microscope. Crista ampullaris was also dissected from 10-weeks-old CBA/J mice and bathed in L-15 medium. The tissue was attached to the bottom of the chamber by the weight of two thin platinum rods (0.5 mm in diameter). The tissue was mounted with the cilia or hair bundles facing upward toward the water-immersion objective. The cilia and hair bundles were imaged using a 63x water immersion objective (Leica) and magnified by an additional 10x relay lens. Ciliary motion was measured and calibrated by a photodiode-based measurement system mounted on the Leica upright microscope(Jia and He, 2005). The magnified image of the cilia was projected onto a photodiode through a rectangular slit. Cilia/bundle motion modulated the light influx to the photodiode. The photocurrent response was calibrated to displacement units by moving the slit a fixed distance (0.5 μm) with the image of the cell in front of the photodiode. After amplification, the photocurrent signal was low pass-filtered by an antialiasing filter before being digitized by a 16-bit A/D board (Digidata 1550A; Molecular Devices). The motile responses were low-pass filtered at 250 Hz and digitized at 1 kHz. Ciliary motion was acquired in a two-second window for each trial and 20 trials were captured for each cell in one recording. The power spectrum of the response was averaged and analyzed in the frequency domain using Clampfit software (version 10, Molecular Devices). The experiments were performed at room temperature (22±2°C).

7. Predicted model of the 96-nm modular repeat in adult vestibular kinocilia

The 96 nm repeat of the human respiratory doublet microtubule and associated axonemal complexes (PDB: 8J07) was utilized as a structural reference to model the 96 nm repeat of the vestibular kinocilia axoneme. Candidate genes associated with the 96 nm repeat—identified through transcriptomic profiling (Table 1) of vestibular HCs—were annotated and mapped to their respective structural compartments based on known or predicted protein localizations within the reference model. Model prediction and visualization were performed using ChimeraX 1.6.1 (Pettersen et al., 2021).

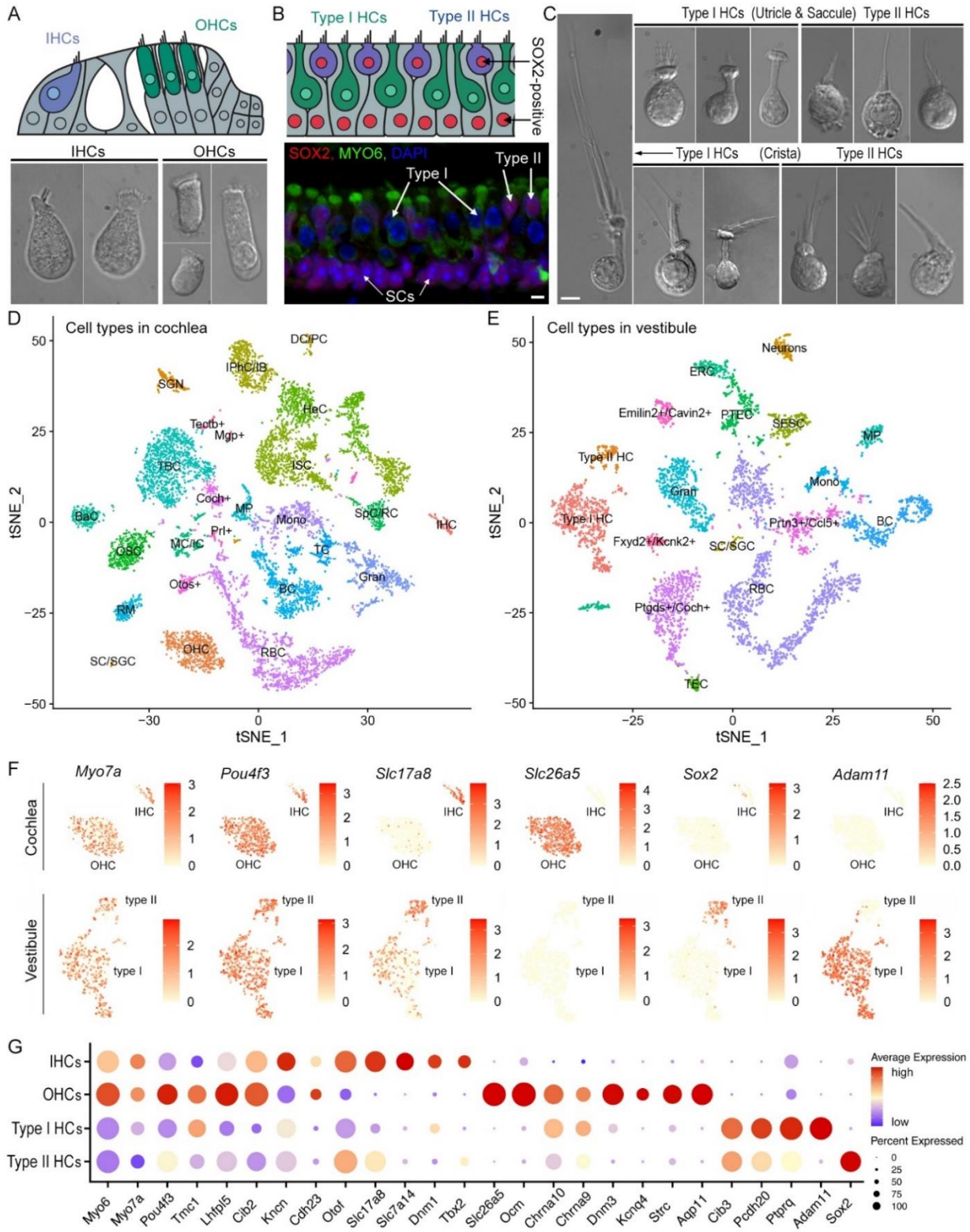

Figure 1: Single-cell transcriptional atlas of cochlear and vestibular cells. **A**: Schematic drawing of the organ of Corti (top panel) and representative images of IHCs and OHCs from adult mouse cochleae. **B**: Schematic drawing of the utricle (top panel) and confocal images of the utricle prepared from an adult mouse. HCs are stained with MYO6, SOX2 and DAPI. SOX2-positive

cells include type II HCs and SCs underneath HCs. **C**: Representative images of type I and type II HCs from utricular and saccular maculae as well as crista ampullaris from adult mice. **D**, **E**: tSNE plots of distinct cell types detected in the adult CBA mouse cochlea (D) and utricle, saccule and crista. Different cell types are color-coded. **F**: Feature plots of the expression 6 marker genes in different HC populations. **G**: Dot plot heatmap of average expression and cellular detection rate of 26 representative marker genes in different HC types in cochleae and vestibular end organs. Abbreviations: IHC (inner HC); OHC (outer HC); SGN (spiral ganglion neuron); SC (Schwann cell)/SGC (satellite glial cell); DC (Deiters' cell)/PC (pillar cell); IPhC (inner phalangeal cell)/IB (inner border cell); ISC (inner sulcus cell); HeC (Hensen's cell); SpC (spindle cell)/RC (root cell); MC (marginal cell)/IC (intermediate cell); BaC (basal cell); MP (macrophage); RM (Reissner's membrane); BC (B cell); TC (T cell); Gran (granulocyte); Mono (monocyte); RBC (red blood cell); OSC (outer sulcus cell); TBC (tympanic border cell). Type I HC (type I HC); Type II HC (type II HC); SESC (sensory epithelial SC); TEC (transitional epithelial cell); PTEC (peripheral transitional epithelial cell); ERC (epithelial roof cell). Neurons (vestibular neurons). For those cells whose definite identities cannot be annotated, the top expressed genes were used for identification and annotation. These cells include Tectb^{+}, Mgp^{+}, Coch^{+}, Prl^{+}, Otos^{+}, Emilin2^{+}/Cavin2^{+}, Fxyd2^{+}/Kcnk2^{+}, Prtn3^{+}/Ccl5^{+}, and Ptgds^{+}/Coch^{+}.

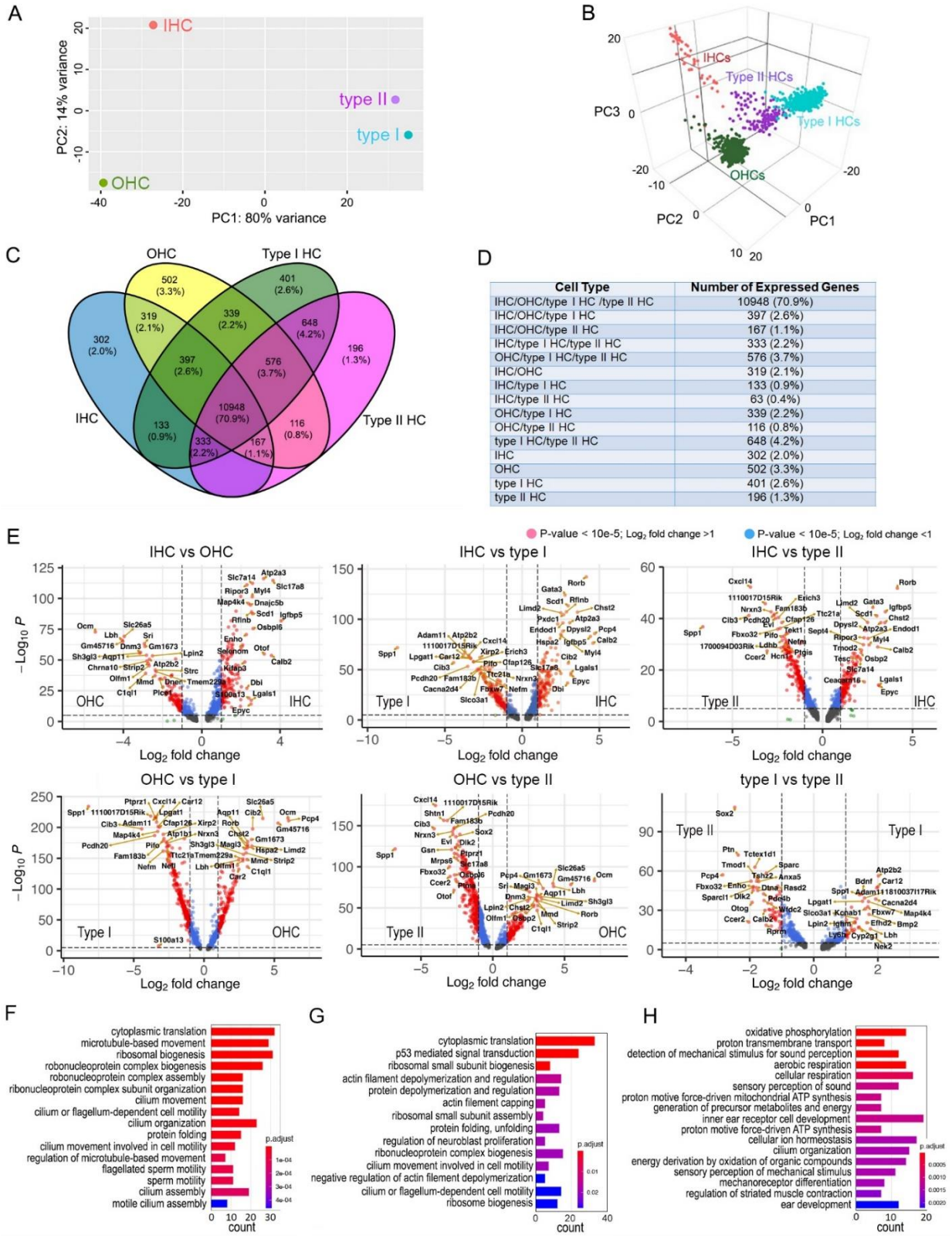

Cell Type	Number of Expressed Genes
IHC/OHC/type I HC /type II HC	10948 (70.9%)
IHC/OHC/type I HC	397 (2.6%)
IHC/OHC/type II HC	167 (1.1%)
IHC/type I HC/type II HC	333 (2.2%)
OHC/type I HC/type II HC	576 (3.7%)
IHC/OHC	319 (2.1%)
IHC/type I HC	133 (0.9%)
IHC/type II HC	63 (0.4%)
OHC/type I HC	339 (2.2%)
OHC/type II HC	116 (0.8%)
type I HC/type II HC	648 (4.2%)
IHC	302 (2.0%)
OHC	502 (3.3%)
type I HC	401 (2.6%)
type II HC	196 (1.3%)

Figure 2: Similarity and difference among different HC types and biological processes enriched in cochlear and vestibular HCs. **A**: PCA plot showing similarity based on pseudo bulk RNA-seq data from four HC types. **B**: PCA plot showing similarity based on individual HC gene expression

among the four HC types. Volcano plot showing differentially expressed genes between different HC types. Red dots indicate differentially expressed genes with P-value < 10^{e}-5 and log_2 fold change > 1. Only the top 20 differentially expressed genes are labeled. **C**: Venn diagram depicting the number of expressed genes (RPKM > 0) in four HC types. **D**: the number and percentage of the total genes shared among two or more cell types or those uniquely expressed by a single cell type. **E**: DEGs identified based on the comparison between different HC types. Only the top 20 genes in each HC type are highlighted. **F**: Biological processes enriched in vestibular HCs compared to cochlear HCs. **G**: Biological processes enriched in type I HCs compared to type II HCs. **H**: Biological processes enriched in type II HCs compared to type I HCs.

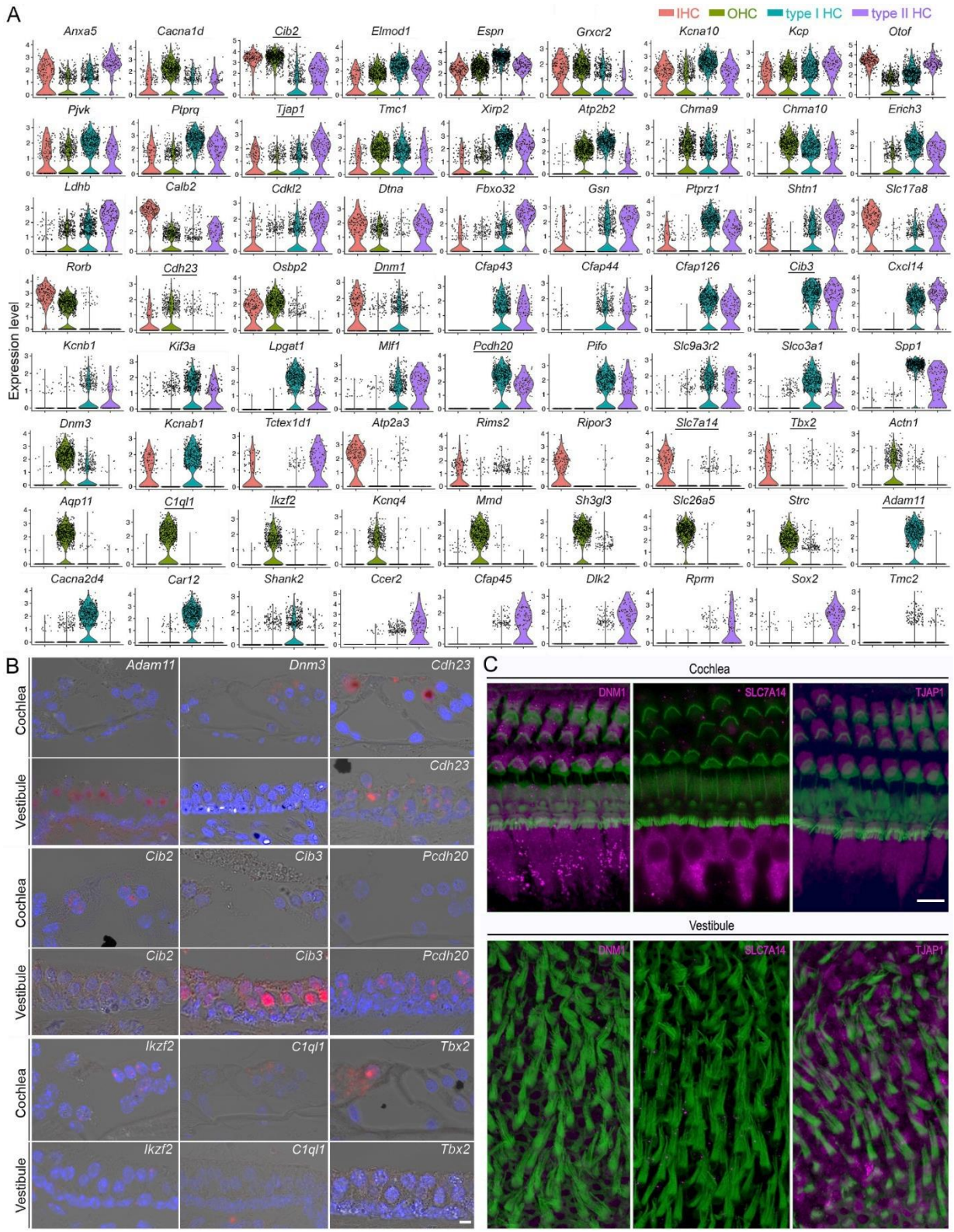

Figure 3: Marker genes and validation of gene expression in cochlear and vestibular HCs. A: Violin plots of gene expression in four different HC types. Expression of the genes with underline is validated in smFISH shown in B. The 72 genes include some that are commonly expressed in all HCs and some that are expressed in three, two, or one HC type(s). **B**: Images from smFISH

showing differential expression of 9 genes in cochlear and vestibular HCs in thin section. Bar: 5 µm for all images in B. **C**: Confocal images of expression of DNM1, SLC7A14, and TJAP1 in cochlear and vestibular HCs. Bar: 10 µm for all images in C.

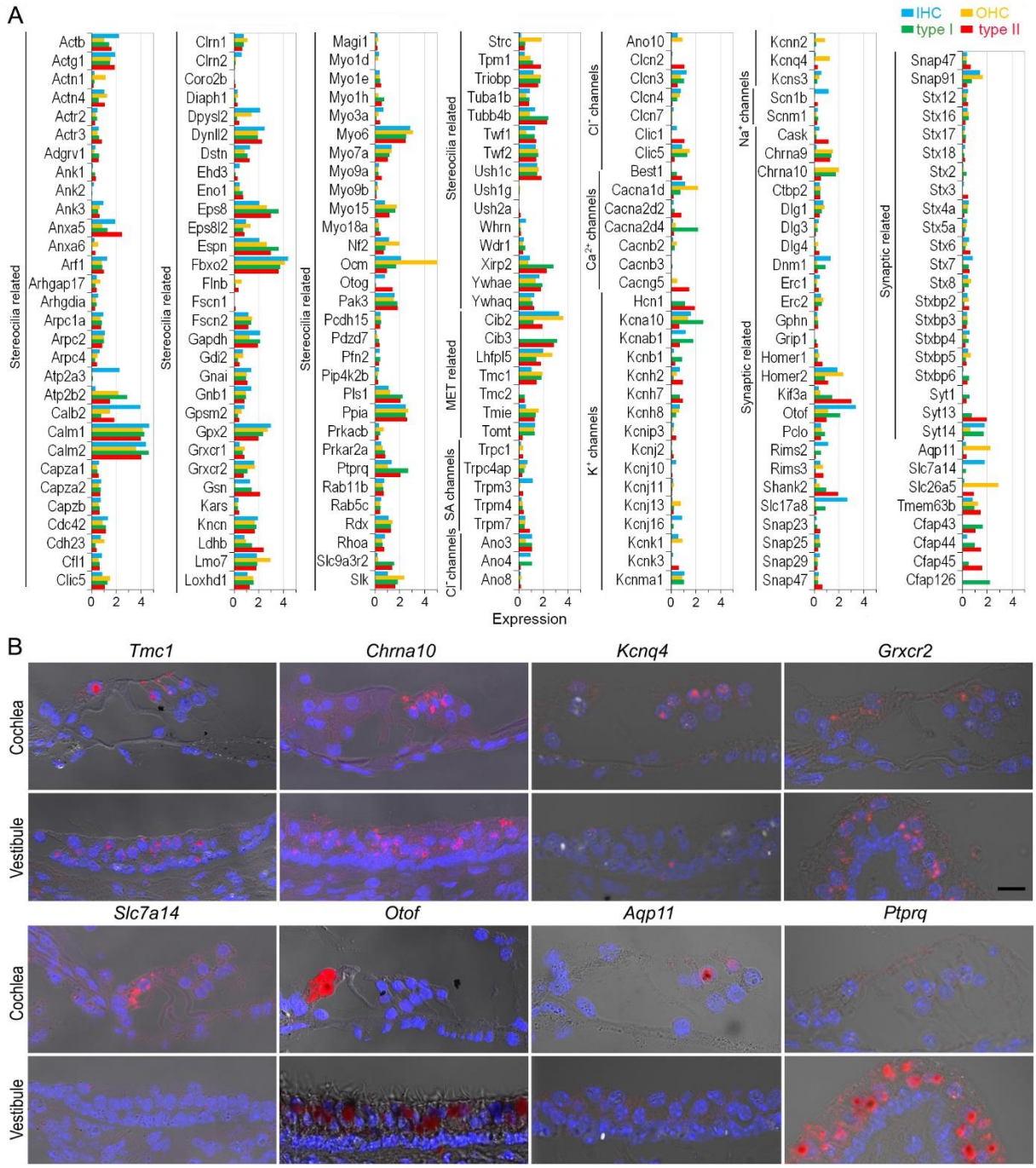

Figure 4: Expression of genes related to HC specialization. **A**: Heatmap showing expression of genes related to stereocilia bundles, mechanotransduction, ion channels and synaptic structure. **B**: Validation of gene expression using smFISH. Bar: 5 µm.

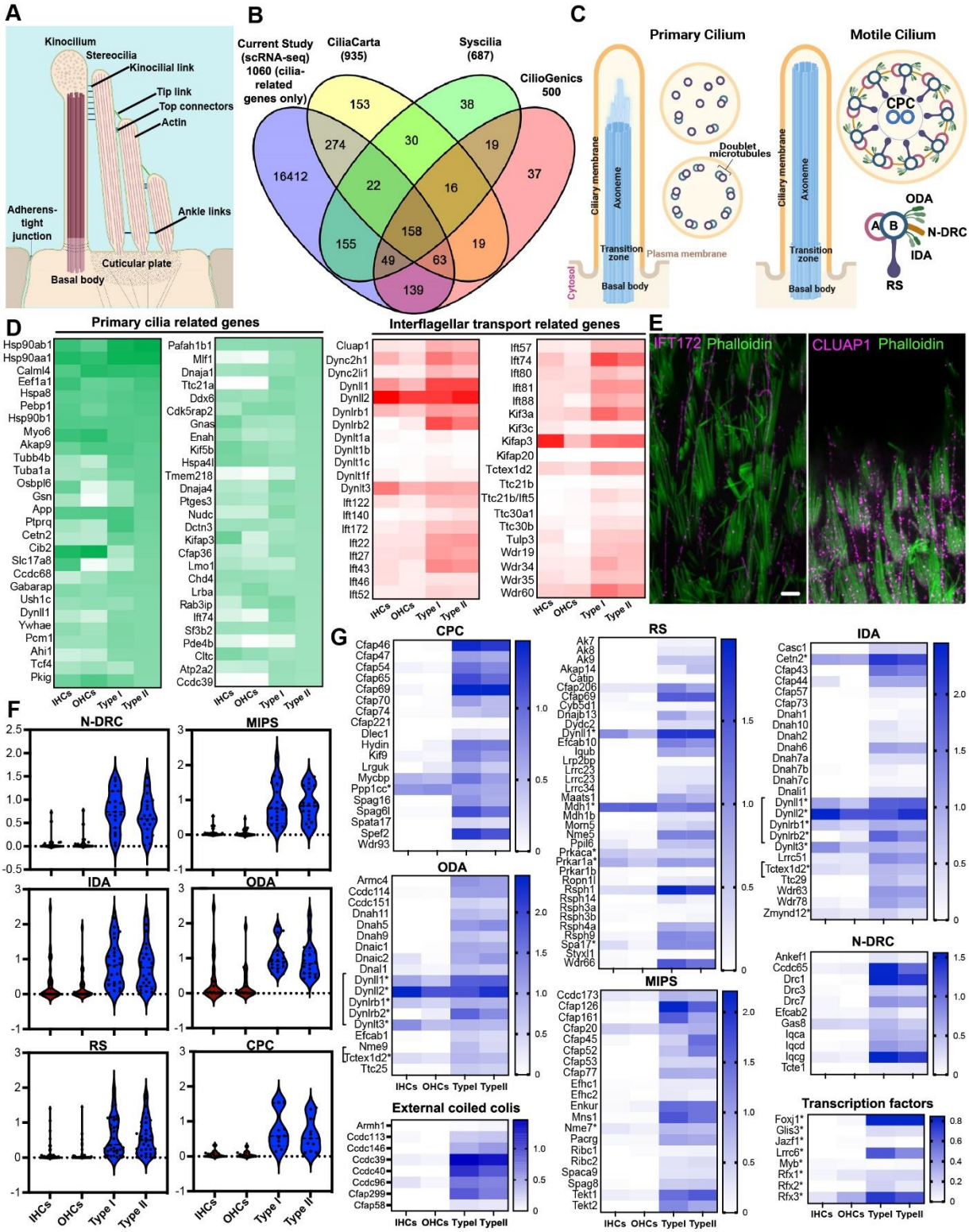

Figure 5. Cilia-related genes detected in cochlear and vestibular HCs. **A:** Schematic illustration of HC hair bundle (adapted from Schwander et al., 2010). **B**: Venn diagram illustrating the number

of genes in each database and the cilia-related genes detected in HC transcriptomes. **C**: Schematic illustration of primary and motile cilia, highlighting 9+0 or 9+2 arrangement of microtubules for primary and motile cilia, respectively: radial spokes (RS), central pair complex (CPC), nexin–dynein regulatory complex (N-DRC), microtubule inner proteins (MIPs), inner and outer dynein arms (IDA and ODA). **D**: Expression of top 50 cilia-related genes and genes related to IFT in the four types of HCs. **E**: Immunostaining of IFT172 and CLUAP1 expression in vestibular kinocilia. Bar: 5 μm. **F**: Violin plots showing aggregated expression of genes associated with 96-nm repeat. **G**: Heatmaps showing the comparison of gene expression related to motile-cilia machinery: radial spokes (RS), central pair complex (CPC), nexin–dynein regulatory complex (N-DRC), microtubule inner proteins (MIPs), inner and outer dynein arms (IDA and ODA), external coiled coils, and motile cilia transcriptional regulators in cochlear and vestibular HCs.

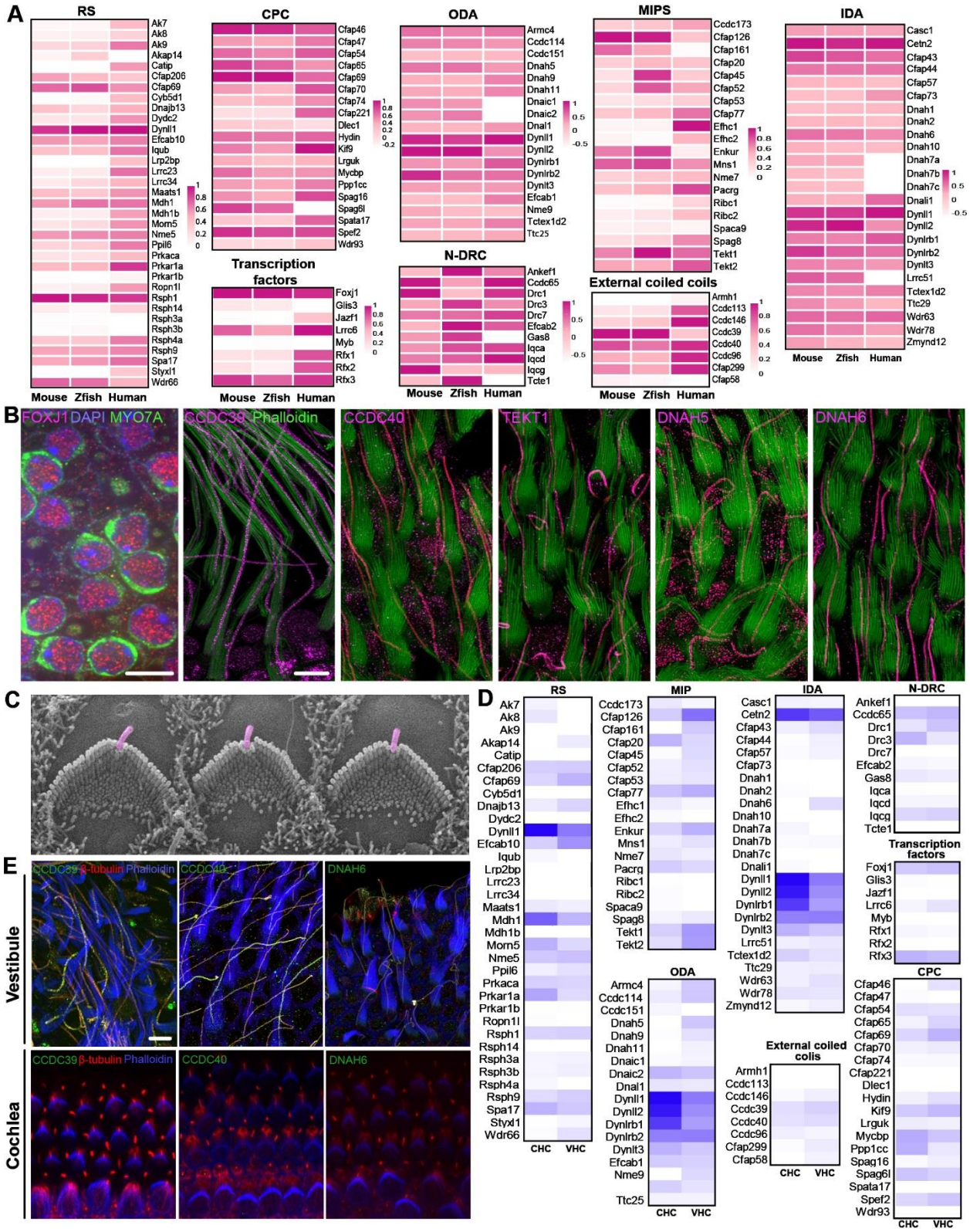

Figure 6: Expression of motile cilia-related genes/proteins in the vestibular HCs. **A:** Expression of motile cilia-related genes in mouse, zebrafish, and human vestibular HCs. Mouse gene nomenclature is used in the heatmaps. **B:** Confocal images of the expression of key motile cilia-

related proteins. Scale bars represent 5 μm. **C**: SEM micrograph of hair bundles of OHCs from P2 cochlea. Kinocilia (in magenta) are still present at this age. **D:** Comparison of expression of motile cilia-related genes between P2 cochlear and vestibular HCs. **E:** Confocal images of expression of CCDC39, CCDC40 and DNAH6 in P2 vestibular and cochlear HCs. CCDC39, CCDC40, and DNAH6 were not expressed in cochlear HCs at P2. Bar: 5 μm.

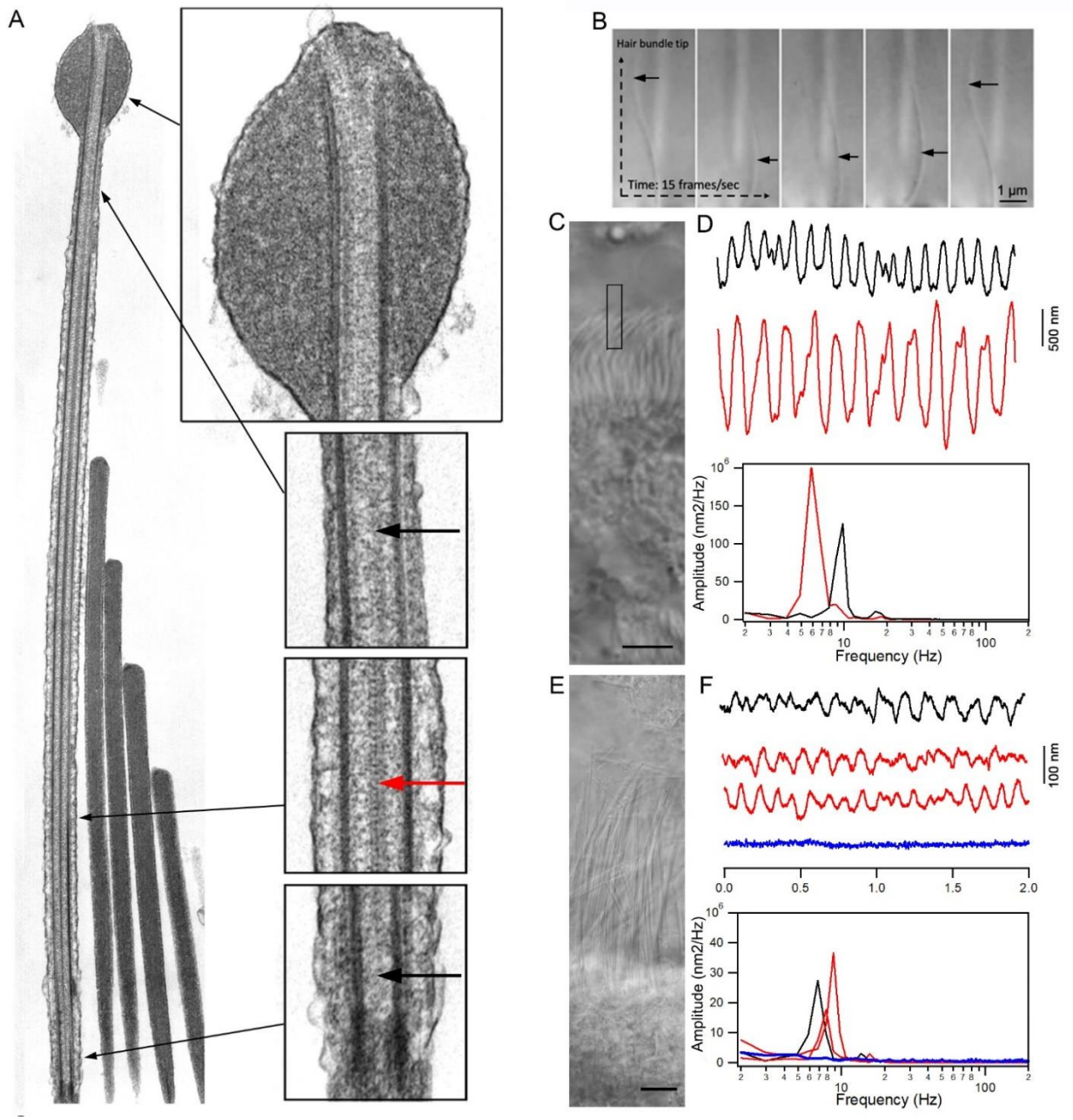

Figure 7: Kinocilia morphology and motility. **A**: TEM images of stereocilia and kinocilium from bullfrog saccular HCs. Different regions of the kinocilium in high magnification are also shown. Long black arrows indicate where the magnified images were taken. Bar: 250 nm. Red arrow indicates two central microtubule singlets. Short black arrows mark absence of central microtubule singlets in the distal regions near the tip of kinocilium and transition zone. **B**: Images captured from *in vitro* live imaging of kinocilium and bundle motion of a bullfrog saccular HC. The images were captured with speed of 15 frames per second. Black arrows indicate kinocilium. **C**: DIC image of cilia from mouse middle ear. Black frame marks where the motion was measured. Bar: 5 µm. **D**: Representative waveforms of spontaneous ciliary motion from middle ear tissue. The FFT analysis of cilia motion is also shown. **E:** DIC image of hair bundles from mouse crista HCs. Bar: 10 µm. **F**: Three representative waveforms of spontaneous motion of hair bundles. The response in blue shows measurements taken from a hair bundle with no motility. Time scale in F

also applies to D. FFT analysis of bundle motion is also shown. Response waveforms and spectra are color-coded and -matched.

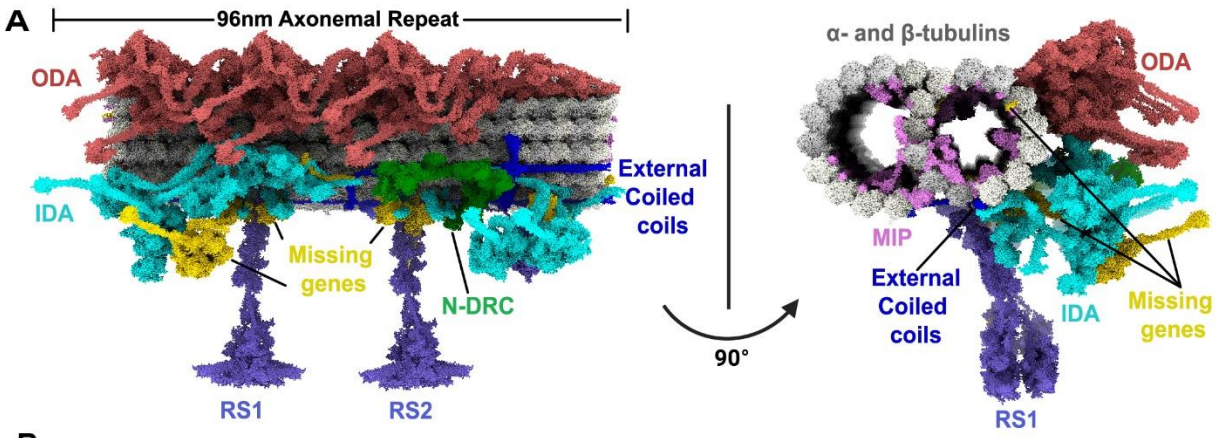

B

Components of the axonemal complex	Missing genes related to axonemal complex	Effect on motility	Cilia-related diseases
IDA	DNAH3	Reduced sperm motility (mouse and human)	Male infertility MMAF (mouse and human)
	DNAH12	Sperm immotility	Male infertility MMAF (mouse and human)
	ACTA2	Unknown	Unknown
	CFAP100/CCDC37	Unknown	Unknown
MIP	CFAP68	Unknown	Unknown
	CFAP90	Unknown	Unknown
	CFAP95	Unknown	Unknown
	CFAP107	Unknown	Unknown
	CFAP141	Unknown	Unknown
	CFAP276	Unknown	Unknown
	FAM166B	Unknown	Unknown
	FAM183A	Unknown	Unknown
	FAM166C	Unknown	Unknown
	Pierce1	KO exhibit ciliary motility and laterality defects (zebrafish)	LR asymmetry (mouse/zebrafish)
	Pierce2	KO exhibit ciliary motility and laterality defects (zebrafish)	LR asymmetry (zebrafish)
RS	MORN3	Unknown	Unknown

Figure 8: Predicted model of the molecular architecture of 96 nm axonemal repeat of vestibular kinocilia. **A**: Longitudinal and cross-sectional views of the doublet microtubule and associated structure in 96-nm repeat, derived from combining cryo-EM data and single-cell transcriptomic analysis. Key axonemal motile-machinery components are color-coded: ODA (orange), IDA (cyan), N-DRC (green), MIPs (pink), RS (purple), and external coiled-coils (blue). Radial spoke 3 (RS3) has not been resolved to atomic resolution, but its shorter form (RS3s) is depicted. α- and

β-tubulins are represented in gray. Regions highlighted in gold indicate the absence of corresponding transcripts in our mouse transcriptomic data. **B**: 16 genes not detected in mouse and human vestibular HC transcriptomes. The roles of these genes in the 96-nm repeat module and cilia motility and ciliopathy are also included in the table.

REFERENCE

Anvarian, Z., Mykytyn, K., Mukhopadhyay, S., Pedersen, L.B., Christensen, S.T., 2019. Cellular signalling by primary cilia in development, organ function and disease. Nat. Rev. Nephrol. 15, 199–219. https://doi.org/10.1038/s41581-019-0116-9

Baird, R.A., 1994. Comparative transduction mechanisms of hair cells in the bullfrog utriculus. II. Sensitivity and response dynamics to hair bundle displacement. J. Neurophysiol. 71, 685–705. https://doi.org/10.1152/jn.1994.71.2.685

Barta, C.L., Liu, H., Chen, L., Giffen, K.P., Li, Y., Kramer, K.L., Beisel, K.W., He, D.Z., 2018. RNA-seq transcriptomic analysis of adult zebrafish inner ear hair cells. Sci. Data 5, 180005. https://doi.org/10.1038/sdata.2018.5

Becker-Heck, A., Zohn, I.E., Okabe, N., Pollock, A., Lenhart, K.B., Sullivan-Brown, J., McSheene, J., Loges, N.T., Olbrich, H., Haeffner, K., Fliegauf, M., Horvath, J., Reinhardt, R., Nielsen, K.G., Marthin, J.K., Baktai, G., Anderson, K.V., Geisler, R., Niswander, L., Omran, H., Burdine, R.D., 2011. The coiled-coil domain containing protein CCDC40 is essential for motile cilia function and left-right axis formation. Nat. Genet. 43, 79–84. https://doi.org/10.1038/ng.727

Benser, M.E., Marquis, R.E., Hudspeth, A.J., 1996. Rapid, Active Hair Bundle Movements in Hair Cells from the Bullfrog's Sacculus. J. Neurosci. 16, 5629–5643. https://doi.org/10.1523/JNEUROSCI.16-18-05629.1996

Brownell, W.E., Bader, C.R., Bertrand, D., de Ribaupierre, Y., 1985. Evoked mechanical responses of isolated cochlear outer hair cells. Science 227, 194–196. https://doi.org/10.1126/science.3966153

Burns, J.C., Kelly, M.C., Hoa, M., Morell, R.J., Kelley, M.W., 2015. Single-cell RNA-Seq resolves cellular complexity in sensory organs from the neonatal inner ear. Nat. Commun. 6, 8557. https://doi.org/10.1038/ncomms9557

Chen, Z., Shiozaki, M., Haas, K.M., Skinner, W.M., Zhao, S., Guo, C., Polacco, B.J., Yu, Z., Krogan, N.J., Lishko, P.V., Kaake, R.M., Vale, R.D., Agard, D.A., 2023. De novo protein identification in mammalian sperm using in situ cryoelectron tomography and AlphaFold2 docking. Cell 186, 5041-5053.e19. https://doi.org/10.1016/j.cell.2023.09.017

Choksi, S.P., Lauter, G., Swoboda, P., Roy, S., 2014. Switching on cilia: transcriptional networks regulating ciliogenesis. Development 141, 1427–1441. https://doi.org/10.1242/dev.074666

Crawford, A.C., Fettiplace, R., 1985. The mechanical properties of ciliary bundles of turtle cochlear hair cells. J. Physiol. 364, 359–379. https://doi.org/10.1113/jphysiol.1985.sp015750

Dallos, P., Wu, X., Cheatham, M.A., Gao, J., Zheng, J., Anderson, C.T., Jia, S., Wang, X., Cheng, W.H.Y., Sengupta, S., He, D.Z.Z., Zuo, J., 2008. Prestin-Based Outer Hair Cell Motility Is Necessary for Mammalian Cochlear Amplification. Neuron 58, 333–339. https://doi.org/10.1016/j.neuron.2008.02.028

Dam, T.J.P. van, Kennedy, J., Lee, R. van der, Vrieze, E. de, Wunderlich, K.A., Rix, S., Dougherty, G.W., Lambacher, N.J., Li, C., Jensen, V.L., Leroux, M.R., Hjeij, R., Horn, N., Texier, Y., Wissinger, Y., Reeuwijk, J. van, Wheway, G., Knapp, B., Scheel, J.F., Franco, B., Mans, D.A., Wijk, E. van, Képès, F., Slaats, G.G., Toedt, G., Kremer, H., Omran, H., Szymanska, K., Koutroumpas, K., Ueffing, M., Nguyen, T.-M.T., Letteboer, S.J.F., Oud, M.M., Beersum, S.E.C. van, Schmidts, M., Beales, P.L., Lu, Q., Giles, R.H., Szklarczyk, R., Russell, R.B., Gibson, T.J., Johnson, C.A., Blacque, O.E., Wolfrum, U., Boldt, K., Roepman, R., Hernandez-Hernandez, V., Huynen, M.A., 2019. CiliaCarta: An integrated and validated compendium of ciliary genes. PLOS ONE 14, e0216705. https://doi.org/10.1371/journal.pone.0216705

Denk, W., Webb, W.W., 1992. Forward and reverse transduction at the limit of sensitivity studied by correlating electrical and mechanical fluctuations in frog saccular hair cells. Hear. Res. 60, 89–102. https://doi.org/10.1016/0378-5955(92)90062-R

Eatock, R.A., Rüsch, A., Lysakowski, A., Saeki, M., 1998. Hair Cells in Mammalian Utricles. Otolaryngol. Neck Surg. 119, 172–181. https://doi.org/10.1016/S0194-5998(98)70052-X

Eatock, R.A., Songer, J.E., 2011. Vestibular Hair Cells and Afferents: Two Channels for Head Motion Signals. Annu. Rev. Neurosci. 34, 501–534. https://doi.org/10.1146/annurev-neuro-061010-113710

Erickson, T., Biggers, W.P., Williams, K., Butland, S.E., Venuto, A., 2023. Regionalized Protein Localization Domains in the Zebrafish Hair Cell Kinocilium. J. Dev. Biol. 11, 28. https://doi.org/10.3390/jdb11020028

Flock, Å., Flock, B., Murray, E., 1977. Studies on the Sensory Hairs of Receptor Cells in the Inner Ear. Acta Otolaryngol. (Stockh.) 83, 85–91. https://doi.org/10.3109/00016487709128817

Ge, S.X., Jung, D., Yao, R., 2020. ShinyGO: a graphical gene-set enrichment tool for animals and plants. Bioinformatics 36, 2628–2629. https://doi.org/10.1093/bioinformatics/btz931

Giffen, K.P., Liu, H., Yamane, K.L., Li, Y., Chen, L., Kramer, K.L., Zallocchi, M., He, D.Z., 2024. Molecular specializations underlying phenotypic differences in inner ear hair cells of zebrafish and mice. Front. Neurol. 15. https://doi.org/10.3389/fneur.2024.1437558

Gui, M., Farley, H., Anujan, P., Anderson, J.R., Maxwell, D.W., Whitchurch, J.B., Botsch, J.J., Qiu, T., Meleppattu, S., Singh, S.K., Zhang, Q., Thompson, J., Lucas, J.S., Bingle, C.D., Norris, D.P., Roy, S., Brown, A., 2021. *De novo* identification of mammalian ciliary motility proteins using cryo-EM. Cell 184, 5791-5806.e19. https://doi.org/10.1016/j.cell.2021.10.007

Hansen, J.N., Sun, H., Kahnert, K., Westenius, E., Johannesson, A., Tzavlaki, K., Winsnes, C., Pohjanen, E., Fall, J., Navarro, F.B., Bäckström, A., Lindskog, C., Johansson, F., Von Feilitzen, K., Vega, A.D., Uhlén, M., Casals, A.M., Mahdessian, D., Lindstrand, A., Axelsson, U., Lundberg, E., 2024. Intrinsic Diversity In Primary Cilia Revealed Through Spatial Proteomics. https://doi.org/10.1101/2024.10.20.619273

Hong, J., Lee, C., Papoulas, O., Pan, J., Takagishi, M., Manzi, N., Dickinson, D.J., Horani, A., Brody, S.L., Marcotte, E., Park, T.J., Wallingford, J.B., 2025. Molecular organization of the distal tip of vertebrate motile cilia. https://doi.org/10.1101/2025.02.19.639145

Howard, J., Hudspeth, A.J., 1987. Mechanical relaxation of the hair bundle mediates adaptation in mechanoelectrical transduction by the bullfrog's saccular hair cell. Proc. Natl. Acad. Sci. 84, 3064–3068. https://doi.org/10.1073/pnas.84.9.3064

Jaeger, R.G., Fex, J., Kachar, B., 1994. Structural basis for mechanical transduction in the frog vestibular sensory apparatus: II. The role of microtubules in the organization of the cuticular plate. Hear. Res. 77, 207–215. https://doi.org/10.1016/0378-5955(94)90268-2

Jan, T.A., Eltawil, Y., Ling, A.H., Chen, L., Ellwanger, D.C., Heller, S., Cheng, A.G., 2021. Spatiotemporal dynamics of inner ear sensory and non-sensory cells revealed by single-cell transcriptomics. Cell Rep. 36, 109358. https://doi.org/10.1016/j.celrep.2021.109358

Jia, S., Dallos, P., He, D.Z.Z., 2007. Mechanoelectric Transduction of Adult Inner Hair Cells. J. Neurosci. 27, 1006–1014. https://doi.org/10.1523/JNEUROSCI.5452-06.2007

Jia, S., He, D.Z.Z., 2005. Motility-associated hair-bundle motion in mammalian outer hair cells. Nat. Neurosci. 8, 1028–1034. https://doi.org/10.1038/nn1509

Kachar, B., Brownell, W.E., Altschuler, R., Fex, J., 1986. Electrokinetic shape changes of cochlear outer hair cells. Nature 322, 365–368. https://doi.org/10.1038/322365a0

Kachar, B., Parakkal, M., Fex, J., 1990. Structural basis for mechanical transduction in the frog vestibular sensory apparatus: I. The otolithic membrane. Hear. Res. 45, 179–190. https://doi.org/10.1016/0378-5955(90)90119-A

Kikuchi, T., Takasaka, T., Tonosaki, A., Watanabe, H., 1989. Fine structure of guinea pig vestibular kinocilium. Acta Otolaryngol. (Stockh.) 108, 26–30. https://doi.org/10.3109/00016488909107388

Kindt, K.S., Finch, G., Nicolson, T., 2012. Kinocilia Mediate Mechanosensitivity in Developing Zebrafish Hair Cells. Dev. Cell 23, 329–341. https://doi.org/10.1016/j.devcel.2012.05.022

Lagziel, A., Ahmed, Z.M., Schultz, J.M., Morell, R.J., Belyantseva, I.A., Friedman, T.B., 2005. Spatiotemporal pattern and isoforms of cadherin 23 in wild type and *waltzer* mice during inner ear hair cell development. Dev. Biol. 280, 295–306. https://doi.org/10.1016/j.ydbio.2005.01.015

Legal, T., Joachimiak, E., Parra, M., Peng, W., Tam, A., Black, C., Valente-Paterno, M., Brouhard, G., Gaertig, J., Wloga, D., Bui, K.H., 2024. Structure of the ciliary tip central pair reveals the unique role of the microtubule-seam binding protein SPEF1. https://doi.org/10.1101/2024.12.02.626492

Legal, T., Parra, M., Tong, M., Black, C.S., Joachimiak, E., Valente-Paterno, M., Lechtreck, K., Gaertig, J., Bui, K.H., 2023. CEP104/FAP256 and associated cap complex maintain stability of the ciliary tip. J. Cell Biol. 222, e202301129. https://doi.org/10.1083/jcb.202301129

Leibovici, M., Verpy, E., Goodyear, R.J., Zwaenepoel, I., Blanchard, S., Lainé, S., Richardson, G.P., Petit, C., 2005. Initial characterization of kinocilin, a protein of the hair cell kinocilium. Hear. Res. 203, 144–153. https://doi.org/10.1016/j.heares.2004.12.002

Leung, M.R., Sun, C., Zeng, J., Anderson, J.R., Niu, Q., Huang, W., Noteborn, W.E.M., Brown, A., Zeev-Ben-Mordehai, T., Zhang, R., 2025. Structural diversity of axonemes across mammalian motile cilia. Nature 1–8. https://doi.org/10.1038/s41586-024-08337-5

Li, Y., Liu, H., Giffen, K.P., Chen, L., Beisel, K.W., He, D.Z.Z., 2018. Transcriptomes of cochlear inner and outer hair cells from adult mice. Sci. Data 5, 180199. https://doi.org/10.1038/sdata.2018.199

Liberman, M.C., Gao, J., He, D.Z.Z., Wu, X., Jia, S., Zuo, J., 2002. Prestin is required for electromotility of the outer hair cell and for the cochlear amplifier 419, 5.

Ma, Y., He, J., Li, S., Yao, D., Huang, C., Wu, J., Lei, M., 2023. Structural insight into the intraflagellar transport complex IFT-A and its assembly in the anterograde IFT train. Nat. Commun. 14, 1506. https://doi.org/10.1038/s41467-023-37208-2

Martin, P., Bozovic, D., Choe, Y., Hudspeth, A.J., 2003. Spontaneous Oscillation by Hair Bundles of the Bullfrog's Sacculus. J. Neurosci. 23, 4533–4548. https://doi.org/10.1523/JNEUROSCI.23-11-04533.2003

Meng, G.-Q., Wang, Y., Luo, C., Tan, Y.-M., Li, Y., Tan, C., Tu, C., Zhang, Q.-J., Hu, L., Zhang, H., Meng, L.-L., Liu, C.-Y., Deng, L., Lu, G.-X., Lin, G., Du, J., Tan, Y.-Q., Sha, Y., Wang, L., He, W.-B., 2024. Bi-allelic variants in DNAH3 cause male infertility with asthenoteratozoospermia in humans and mice. Hum. Reprod. Open 2024, hoae003. https://doi.org/10.1093/hropen/hoae003

Merveille, A.-C., Davis, E.E., Becker-Heck, A., Legendre, M., Amirav, I., Bataille, G., Belmont, J., Beydon, N., Billen, F., Clément, A., Clercx, C., Coste, A., Crosbie, R., de Blic, J., Deleuze, S., Duquesnoy, P., Escalier, D., Escudier, E., Fliegauf, M., Horvath, J., Hill, K., Jorissen, M., Just, J., Kispert, A., Lathrop, M., Loges, N.T., Marthin, J.K., Momozawa, Y., Montantin, G., Nielsen, K.G., Olbrich, H., Papon, J.-F., Rayet, I., Roger, G., Schmidts, M., Tenreiro, H., Towbin, J.A., Zelenika, D., Zentgraf, H., Georges, M., Lequarré, A.-S., Katsanis, N., Omran, H., Amselem, S., 2011. CCDC39 is required for assembly of inner dynein arms and the dynein regulatory complex and for normal ciliary motility in humans and dogs. Nat. Genet. 43, 72–78. https://doi.org/10.1038/ng.726

Moon, K.-H., Ma, J.-H., Min, H., Koo, H., Kim, H., Ko, H.W., Bok, J., 2020. Dysregulation of sonic hedgehog signaling causes hearing loss in ciliopathy mouse models. eLife 9, e56551. https://doi.org/10.7554/eLife.56551

Nagel, Z.D., Margulies, C.M., Chaim, I.A., McRee, S.K., Mazzucato, P., Ahmad, A., Abo, R.P., Butty, V.L., Forget, A.L., Samson, L.D., 2014. Multiplexed DNA repair assays for multiple lesions and multiple doses via transcription inhibition and transcriptional mutagenesis. Proc. Natl. Acad. Sci. 111, E1823–E1832. https://doi.org/10.1073/pnas.1401182111

Oda, T., Yanagisawa, H., Kamiya, R., Kikkawa, M., 2014. A molecular ruler determines the repeat length in eukaryotic cilia and flagella. Science 346, 857–860. https://doi.org/10.1126/science.1260214

O'Donnell, J., Zheng, J., 2022. Vestibular Hair Cells Require CAMSAP3, a Microtubule Minus-End Regulator, for Formation of Normal Kinocilia. Front. Cell. Neurosci. 16.

Pettersen, E.F., Goddard, T.D., Huang, C.C., Meng, E.C., Couch, G.S., Croll, T.I., Morris, J.H., Ferrin, T.E., 2021. UCSF ChimeraX: Structure visualization for researchers, educators, and developers. Protein Sci. 30, 70–82. https://doi.org/10.1002/pro.3943

Pir, M.S., Begar, E., Yenisert, F., Demirci, H.C., Korkmaz, M.E., Karaman, A., Tsiropoulou, S., Firat-Karalar, E.N., Blacque, O.E., Oner, S.S., Doluca, O., Cevik, S., Kaplan, O.I., 2024. CilioGenics: an integrated method and database for predicting novel ciliary genes. Nucleic Acids Res. 52, 8127–8145. https://doi.org/10.1093/nar/gkae554

Ranum, P.T., Goodwin, A.T., Yoshimura, H., Kolbe, D.L., Walls, W.D., Koh, J.-Y., He, D.Z.Z., Smith, R.J.H., 2019. Insights into the Biology of Hearing and Deafness Revealed by Single-Cell RNA Sequencing. Cell Rep. 26, 3160-3171.e3. https://doi.org/10.1016/j.celrep.2019.02.053

Ricci, A.J., Crawford, A.C., Fettiplace, R., 2003. Tonotopic Variation in the Conductance of the Hair Cell Mechanotransducer Channel. Neuron 40, 983–990. https://doi.org/10.1016/S0896-6273(03)00721-9

Roberts, W.M., Howard, J., Hudspeth, A.J., 1988. Hair Cells: Transduction, Tuning, and Transmission in the Inner Ear. Annu. Rev. Cell Dev. Biol. 4, 63–92. https://doi.org/10.1146/annurev.cb.04.110188.000431

Rüsch, A., Thurm, U., 1990. Spontaneous and electrically induced movements of ampullary kinocilia and stereovilli. Hear. Res. 48, 247–263. https://doi.org/10.1016/0378-5955(90)90065-W

Schwander, M., Kachar, B., Müller, U., 2010. The cell biology of hearing. J. Cell Biol. 190, 9–20. https://doi.org/10.1083/jcb.201001138

Shi, H., Wang, H., Zhang, C., Lu, Y., Yao, J., Chen, Z., Xing, G., Wei, Q., Cao, X., 2022. Mutations in OSBPL2 cause hearing loss associated with primary cilia defects via sonic hedgehog signaling [WWW Document]. https://doi.org/10.1172/jci.insight.149626

Shin, J.-B., Krey, J.F., Hassan, A., Metlagel, Z., Tauscher, A.N., Pagana, J.M., Sherman, N.E., Jeffery, E.D., Spinelli, K.J., Zhao, H., Wilmarth, P.A., Choi, D., David, L.L., Auer, M., Barr-Gillespie, P.G., 2013. Molecular architecture of the chick vestibular hair bundle. Nat. Neurosci. 16, 365–374. https://doi.org/10.1038/nn.3312

Spoon, C., Grant, W., 2011. Biomechanics of hair cell kinocilia: experimental measurement of kinocilium shaft stiffness and base rotational stiffness with Euler–Bernoulli and Timoshenko beam analysis. J. Exp. Biol. 214, 862–870. https://doi.org/10.1242/jeb.051151

Stooke-Vaughan, G.A., Huang, P., Hammond, K.L., Schier, A.F., Whitfield, T.T., 2012. The role of hair cells, cilia and ciliary motility in otolith formation in the zebrafish otic vesicle. Development 139, 1777–1787. https://doi.org/10.1242/dev.079947

Sung, Y.H., Baek, I.-J., Kim, Y.H., Gho, Y.S., Oh, S.P., Lee, Y.J., Lee, H.-W., 2016. PIERCE1 is critical for specification of left-right asymmetry in mice. Sci. Rep. 6, 27932. https://doi.org/10.1038/srep27932

Tai, L., Yin, G., Huang, X., Sun, F., Zhu, Y., 2023. In-cell structural insight into the stability of sperm microtubule doublet. Cell Discov. 9, 1–19. https://doi.org/10.1038/s41421-023-00606-3

Vasquez, S.S.V., van Dam, J., Wheway, G., 2021. An updated SYSCILIA gold standard (SCGSv2) of known ciliary genes, revealing the vast progress that has been made in the cilia research field. Mol. Biol. Cell 32, br13. https://doi.org/10.1091/mbc.E21-05-0226

Walton, T., Gui, M., Velkova, S., Fassad, M.R., Hirst, R.A., Haarman, E., O'Callaghan, C., Bottier, M., Burgoyne, T., Mitchison, H.M., Brown, A., 2023. Axonemal structures reveal mechanoregulatory and disease mechanisms. Nature 618, 625–633. https://doi.org/10.1038/s41586-023-06140-2

Wang, D., Zhou, J., 2021. The Kinocilia of Cochlear Hair Cells: Structures, Functions, and Diseases. Front. Cell Dev. Biol. 9. https://doi.org/10.3389/fcell.2021.715037

Wang, T., Ling, A.H., Billings, S.E., Hosseini, D.K., Vaisbuch, Y., Kim, G.S., Atkinson, P.J., Sayyid, Z.N., Aaron, K.A., Wagh, D., Pham, N., Scheibinger, M., Zhou, R., Ishiyama, A., Moore, L.S., Maria, P.S., Blevins, N.H., Jackler, R.K., Alyono, J.C., Kveton, J., Navaratnam, D., Heller, S., Lopez, I.A., Grillet, N., Jan, T.A., Cheng, A.G., 2024. Single-cell transcriptomic atlas reveals increased regeneration in diseased human inner ear balance organs. Nat. Commun. 15, 4833. https://doi.org/10.1038/s41467-024-48491-y

Wilkerson, B.A., Zebroski, H.L., Finkbeiner, C.R., Chitsazan, A.D., Beach, K.E., Sen, N., Zhang, R.C., Bermingham-McDonogh, O., 2021. Novel cell types and developmental lineages revealed by single-cell RNA-seq analysis of the mouse crista ampullaris. eLife 10, e60108. https://doi.org/10.7554/eLife.60108

Wu, D., Freund, J.B., Fraser, S.E., Vermot, J., 2011. Mechanistic Basis of Otolith Formation during Teleost Inner Ear Development. Dev. Cell 20, 271–278. https://doi.org/10.1016/j.devcel.2010.12.006

Yang, M., Hussain, H.M.J., Khan, M., Muhammad, Z., Zhou, J., Ma, A., Huang, X., Ye, J., Chen, M., Zhi, A., Liu, T., Khan, R., Ali, A., Shah, W., Zeb, A., Ahmad, N., Zhang, H., Xu, B., Ma, H., Shi, Q., Shi, B., 2024. Deficiency in a special dynein DNAH12 causes male infertility by impairing DNAH1 and DNALI1 recruitment in humans and mice. eLife 13. https://doi.org/10.7554/eLife.100350.1

Zheng, J., Shen, W., He, D.Z.Z., Long, K.B., Madison, L.D., Dallos, P., 2000. Prestin is the motor protein of cochlear outer hair cells. Nature 405, 149–155. https://doi.org/10.1038/35012009

Acknowledgments
We acknowledge the use of the Auditory and Vestibular Technology (AVT) Core of Translational Hearing Research Center at Creighton University for high-resolution confocal imaging and library preparation (10x Genomics), and the University of Nebraska DNA Sequencing Core Facility for scRNA-seq. The AVT core at Creighton University receives partial support from NIH grant 1P20GM139762-01 from the NIGMS. The University of Nebraska DNA Sequencing Core receives partial support from the NCRR (RR018788). Scanning electron microscope was acquired through a Nebraska EPSCoR MRI award (Creighton-Department of Chemistry & Biochemistry) and was wholly funded by Nebraska EPSCoR. This research was also supported by the NIDCD/NIH Intramural Research Program and utilized the computational resources of the NIH HPC Biowulf cluster (http://hpc.nih.gov). We thank Drs. Marrisa Zallocchi, Justine Renauld, and Sarath Vijayakumar at Creighton University for helpful discussions.

Funding:
National Institutes of Health grant IRP fund Z01-DC000002 from NIDCD (BK)
National Institutes of Health grant R01 DC016807 from NIDCD (DH)

Author contributions: D.H., B.K., and A.T. conceived the project. Z.X., H.L., S.T., Y.L., and D.H. collected the inner ear tissues and prepared the library for scRNA-seq. Z.X., A.T., S.K., C.B., J.Z., L.T., and D.H. performed the bioinformatics analyses. A.T. conducted the structural modeling. A.T., H.L., S.K., D.H., and B.K. carried out the microscopy and physiological experiments. A.T., Z.X., S.K., C.B., B.K., and D.H. contributed to the preparation and editing of the manuscript and figures.

Competing interests: Authors declare that they have no competing interests.

Data and materials availability: Original scRNA-seq data are available (GSE283534). Data are visualized in the main text or the supplementary materials.

Supplementary files include:

Table S1 (Excel file for transcriptomes of four HC types)

Table S2 (Word file for genes associated with 96-nm repeat)

Fig. S1: GO analysis of enriched genes in cellular localization and biological processes primarily related to cilia organization, assembly, maintenance, intracellular transport, and microtubule dynamics particularly associated with motile cilia

Fig. S2: Primary cilia-related genes in four HC types

Fig. S3: Comparison of HC transcriptomes with multi-tissue proteomics datasets

Videos S1 and S2: Bullfrog kinocilia motility